



Nordisk kernesikkerhedsforskning
Norrænar kjarnöryggisrannsóknir
Pohjoismainen ydinturvallisuustutkimus
Nordisk kjernesikkerhetsforskning
Nordisk kärnsäkerhetsforskning
Nordic nuclear safety research

NKS-127
ISBN 87-7893-189-4

Fluid-Structure Interaction Analysis of a Water Pool under Loading Caused by Steam Injection

Antti Timperi, Timo Pätkängas, Jarto Niemi and Mikko Ilvonen
VTT Technical Research Centre of Finland

April 2006

Abstract

Fluid-structure interaction (FSI) calculations were carried out by coupling CFD and structural analysis codes. MpCCI 3.0 was used for coupling Fluent CFD code with ABAQUS FE code. ES-FSI was used for coupling Star-CD CFD code with ABAQUS. FSI analyses, in which the calculation was carried out entirely in ABAQUS, were also performed. In this case, acoustic elements were used for the fluid and the acoustic and structural domains were coupled. FSI calculations were performed for simple test cases and for a test pool at Lappeenranta University of Technology. The Method of Images was studied as an alternative method for the analyses of the pool. Particularly, the determination of pressure source for the method was studied. Earlier work carried out with the homogenous two-phase model was continued by testing the model with Fluent. Calculation of condensation of steam in a water pool was tested with a new implementation.

The two-directionally coupled simulations of the pool with MpCCI and ES-FSI were found to be numerically instable. It was concluded that an implicit coupling method may have to be used in order to avoid the instability. Calculations of the pool were finally performed by using one-directional coupling. In the simulations with MpCCI, the incompressible and compressible VOF models of Fluent were used. With ES-FSI, the incompressible VOF model of Star-CD was used for modelling the beginning of a steam injection experiment. The magnitudes of pressure and stress peaks in the simulation and experiment were of comparable size. Otherwise, however, differences between the simulation and experiment were large due to the simplifications used in the simulation. Results obtained with the acoustic-structural FE analyses were compared to analytical and experimental results. The results indicated that the coupled acoustic-structural analysis can be used for calculating the coupled eigenmodes of BWR pressure suppression pools.

Key words

CFD, FE, fluid-structure interaction, steam injection, pressure suppression pool

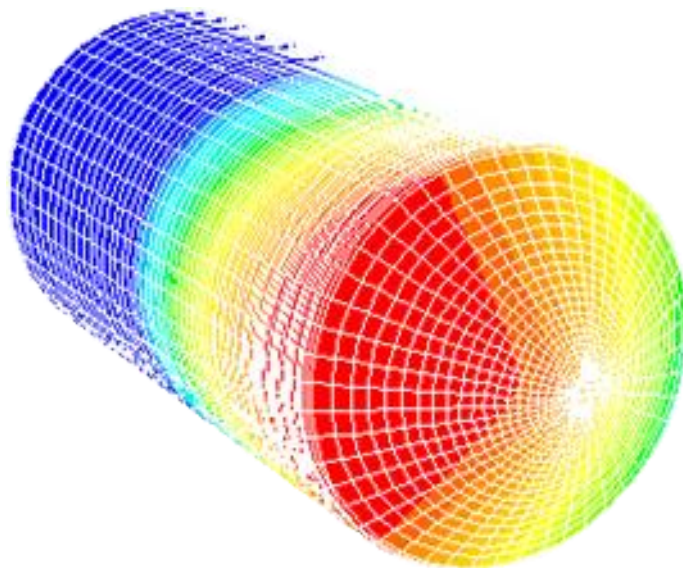
NKS-127

ISBN 87-7893-189-4

Electronic report, April 2006

The report can be obtained from
NKS Secretariat
NKS-775
P.O. Box 49
DK - 4000 Roskilde, Denmark

Phone +45 4677 4045
Fax +45 4677 4046
www.nks.org
e-mail nks@nks.org

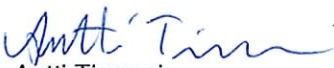


Fluid-Structure Interaction Analysis of a Water Pool under Loading Caused by Steam Injection

Authors Antti Timperi, Timo Pättikangas, Jarto Niemi and Mikko Ilvonen

Confidentiality: Public



Report's title Fluid-Structure Interaction Analysis of a Water Pool under Loading Caused by Steam Injection		
Customer, contact person, address VYR, NKS	Order reference	
Project name SAFIR / INTELI / INPUT	Project number /Short name G5SU01037 / INPUT	
Author(s) Antti Timperi, Timo Pättikangas, Jarto Niemi and Mikko Ilvonen	Pages 64	
Key words CFD, FE, fluid-structure interaction, steam injection, pressure suppression pool	Report identification code TUO72-056662	
<p>Summary</p> <p>Fluid-structure interaction (FSI) calculations were carried out by coupling CFD and structural analysis codes. MpCCI 3.0 was used for coupling Fluent CFD code with ABAQUS FE code. ES-FSI was used for coupling Star-CD CFD code with ABAQUS. FSI analyses, in which the calculation was carried out entirely in ABAQUS, were also performed. In this case, acoustic elements were used for the fluid and the acoustic and structural domains were coupled. FSI calculations were performed for simple test cases and for a test pool at Lappeenranta University of Technology. The Method of Images was studied as an alternative method for the analyses of the pool. Particularly, the determination of pressure source for the method was studied. Earlier work carried out with the homogenous two-phase model was continued by testing the model with Fluent. Calculation of condensation of steam in a water pool was tested with a new implementation.</p> <p>The two-directionally coupled simulations of the pool with MpCCI and ES-FSI were found to be numerically unstable. It was concluded that an implicit coupling method may have to be used in order to avoid the instability. Calculations of the pool were finally performed by using one-directional coupling. In the simulations with MpCCI, the incompressible and compressible VOF models of Fluent were used. With ES-FSI, the incompressible VOF model of Star-CD was used for modelling the beginning of a steam injection experiment. The magnitudes of pressure and stress peaks in the simulation and experiment were of comparable size. Otherwise, however, differences between the simulation and experiment were large due to the simplifications used in the simulation. Results obtained with the acoustic-structural FE analyses were compared to analytical and experimental results. The results indicated that the coupled acoustic-structural analysis can be used for calculating the coupled eigenmodes of BWR pressure suppression pools.</p>		
Confidentiality:	Public	
Espoo 09.03.2006		
Signatures		
		
Liisa Heikinheimo Technology Manager	Antti Timperi Research Scientist	Arja Saarenheimo Checked
VTT's contact address P.O. Box 1000, FI-02044 VTT		
Distribution (customer and VTT): STUK (4), Jesper Kierkegaard (SwedPower), Heikki Sjövall (TVO), Pentti Varpasuo (Fortum Nuclear Services), Ville Lestinen (Fortum Nuclear Services), Markku Puustinen (LUT), Jani Laine (LUT), Heikki Purhonen (LUT), Arja Saarenheimo (VTT), Antti Timperi (VTT), Jarto Niemi (VTT), Timo Pättikangas (VTT), Mikko Ilvonen (VTT), VTT archive		
<p><i>The use of the name of the Technical Research Centre of Finland (VTT) in advertising or publication in part of this report is only permissible by written authorisation from the Technical Research Centre of Finland.</i></p>		

Preface

This study is part of the INTELI (Integrity and Life Time of Reactor Circuits) project carried out in the SAFIR Programme, the Finnish Research Programme on Nuclear Power Plant Safety. This study is partly funded by the State Nuclear Waste Management Fund (VYR) and by the Nordic Nuclear Safety Research (NKS). The contact person in STUK is Dr. Martti Vilpas.

The authors are grateful to the members of the POOLEX project at the Lappeenranta University of Technology, Mr. Jani Laine, Mr. Markku Puustinen and Mr. Heikki Purhonen, for discussions on their experimental results.

Espoo,

Authors

Contents

1	Introduction	5
2	Determination of Pressure Source for the Method of Images	6
2.1	The Chugging Phenomenon	6
2.2	A Brief Literature Survey	8
2.3	Potential Flow	10
2.4	Numerical Solution of Poisson Equation	11
2.5	Method of Images	12
2.6	The Fortran Code moi.f	13
2.7	Determination of the Pressure Source	14
2.7.1	The Method of Wood et al. (1980)	14
2.7.2	Solution of Pressure Source by moi.f	15
2.7.3	Pressure Source from Second Time Derivative of Bubble Volume	15
2.7.4	Pressure Source from Maximum Rate of Change of Bubble Volume	15
2.7.5	Theoretical Expressions for Bubble Volume	15
2.7.6	Experimental Determination of Bubble Volume	17
2.7.7	Pressure Source from the Divergence Theorem	17
2.8	Suggestions for Pressure Source Studies	17
3	Homogeneous Two-phase Model for CFD Calculations	18
3.1	Outline of the Implementation	18
3.1.1	Pressure-Flow Solution	18
3.1.2	Heat Transfer Solution	18
3.2	Test Case	19
3.3	Test Calculations	19
3.3.1	An Explanation for Divergence	21
4	Coupled CFD and Structural Analyses	24
4.1	Fluid-structure calculations with Fluent and ABAQUS	25
4.1.1	Simple Test Case: Box with Flexible Walls	26
4.1.2	Water pool: Stability Issues in Two-directional Coupling	28
4.1.3	Water Pool Simulation with One-directional Coupling	30
4.2	Fluid-structure Calculations with Star-CD and ABAQUS	40
4.2.1	ES-FSI Code	40
4.2.2	CFD and Structural Models	40
4.2.3	Simulation of the POOLEX Experiment	41
4.2.4	Results for One-directional FSI Simulation	42
5	Coupled Acoustic-structural Analyses with ABAQUS	48
5.1	Governing Equations	48
5.2	Effect of Compressibility of the Fluid	48
5.3	Calculations for a Two-dimensional Test Case	49

5.3.1	Problem Description	49
5.3.2	FE Model for ABAQUS Calculations	49
5.3.3	Results of Eigenvalue Extraction	50
5.4	Calculations for a Three-dimensional Test Case	51
5.4.1	Problem Description	51
5.4.2	FE Model for ABAQUS Calculations	51
5.4.3	Results of Eigenvalue Extraction	52
5.5	Calculations for the Pool	55
5.5.1	FE Model	55
5.5.2	Results of Eigenvalue Extraction	55
6	Summary and Conclusions	58
6.1	Method of Images	58
6.2	Homogeneous Two-phase Model	59
6.3	Coupled CFD and Structural Analyses	59
6.4	Coupled Acoustic-structural Analyses	60
	References	62

1 Introduction

In boiling water reactors, understanding the behaviour of the reactor pressure suppression pool during a loss-of-coolant accident (LOCA) is of great importance. In LOCA, considerable loads could occur as large amount of non-condensable gas and steam is injected into the pressure suppression pool. The injection causes different kinds of pressure loads to the pool structures. Periodic or nearly periodic loads are caused by the break-up of bubbles at the blowdown pipe outlet and by the chugging and condensation oscillation phenomena. Severe loads, which may be quasi-periodic as well, are also caused by water hammers induced by rapidly condensing large steam bubbles. Such bubbles may in certain conditions occur near the outlet of the blowdown pipes as pure or nearly pure steam is injected into the pool.

It is necessary to develop computational fluid dynamics (CFD) and other methods for calculating the pressure loads caused by the injection of steam. In calculating the behaviour of the pressure suppression pool, fluid-structure interaction (FSI) phenomena may be important especially in the presence of water hammers. In addition, FSI has to be taken into account in calculating the possible fluid-structural resonance of the suppression pool due to periodic or nearly periodic excitation.

In the POOLEX project of the Finnish Research Programme on Nuclear Power Plant Safety (SAFIR), injection of air and steam into a water pool is investigated experimentally at Lappeenranta University of Technology. In the first experimental series, air was injected into the pool through a vertical pipe submerged in water (Laine, 2002). In the second series, experiments with steam have been conducted (Laine and Puustinen, 2003, 2005).

Previously, FSI analyses of the pool with one-directional and two-directional coupling have been performed. Numerical simulations of the tests with air are presented by Calonius et al. (2003), Pättikangas and Pokela (2003) and Tuomainen (2001). The injection of steam was considered by Timperi et al. (2004) and Pättikangas et al. (2005), where a large rapidly condensing steam bubble was modelled with a single-phase CFD calculation. In the latter of these, a two-directional coupling was used. Also in the MULTIPHYSICS project of the SAFIR programme, LOCA is analysed in a pressurised-water reactor with two-directional FSI calculations. In addition, the Method of Images (MOI) was used for calculating pressure loads in the pool and the homogenous two-phase model was tested for CFD calculations with Star-CD by Pättikangas et al. (2005).

In the present work, FSI calculations of the water pool are carried out with the MpCCI and ES-FSI codes. MpCCI is used for coupling the Fluent CFD code with the ABAQUS finite element (FE) code. The Star-CD CFD code is coupled with ABAQUS by using the internal coupling code ES-FSI of Star-CD. FSI analyses, in which the calculation is carried out entirely in ABAQUS, are also presented. In this case, acoustic elements are used for the fluid and the acoustic and structural domains are coupled. Comparison of some of the calculations to the POOLEX experiments is carried out. In addition, work carried out with the Method of Images (MOI) and the homogenous two-phase model for CFD calculations is presented. The MOI is further studied as an alternative method for the analyses of pressure suppression pools. The main emphasis is on the determination of pressure source for the method. Earlier work performed with the homogenous two-phase model is continued by testing the model with the Fluent code in calculating the condensation of steam in a water pool.

Determination of pressure source for the Method of Images is discussed in Sec. 2. Sec. 3 presents the Fluent implementation of the homogeneous two-phase model and test calculations carried out with the model. The coupled CFD and structural simulations are described in Sec. 4. The coupled acoustic-structural analyses with ABAQUS are presented in Sec. 5. Finally, Sec. 6 contains a summary and discussion on the results.

2 Determination of Pressure Source for the Method of Images

The work reported in this section is direct continuation to that done previously by Timo Narumo and reported in Pättikangas et al. (2005). In that work, an older computer code (moi.f) was converted to run in the current computing environment, and several sample pressure fields for the POOLEX condensation pool were calculated and plotted. The code is an implementation of the Method of Images (MOI) to solve the Poisson equation for pressure. The main objective of the work was (and continues to be) to estimate the pressure loads on the pool inner walls during discharge of steam through a vertical pipe into pool water, most notably in the direct contact condensation (DCC) mode called chugging.

The main question that remained open in the previous work was how to determine the pressure source S (in Pascal meter, $\text{Pa m} = \text{kg/s}^2$) appearing in the numerator of the MOI formula. To be more exact, S is the total strength of the source of the negative pressure gradient vector field $-\text{grad}(p)$; note that the pressure due to chugging in pool water generally increases when approaching the steam bubble. Then, S is related to the source term (right-hand side) s of the Poisson equation for pressure in that S is the volume integral of s , which in turn is called source density (in Pa/m^2). For more detailed formulas, see Eerikäinen (1997).

Main emphasis in this work is on the calculation of the MOI pressure source in chugging. Some consideration is also given to the question whether the MOI is the appropriate solution method or not. Discussion of these topics mainly follows the guidelines given by Lauri Eerikäinen in his related work Eerikäinen (1997). Also, some basic theory and literature survey are briefly presented.

2.1 The Chugging Phenomenon

Steam chugging is a mode of direct contact condensation in cases where steam is injected from a pipe into subcooled water in a pool. This may happen, for example, under certain conditions in boiling water reactors (BWRs), which are equipped with a suppression water pool. With relatively low steam mass fluxes (appr. in the order of $20 \dots 30 \text{ kg/m}^2\text{s}$) and low water temperatures (in the order of $0 \dots 40$ degrees C) an oscillating behavior of the steam-water interface arises; see the condensation mode map below.

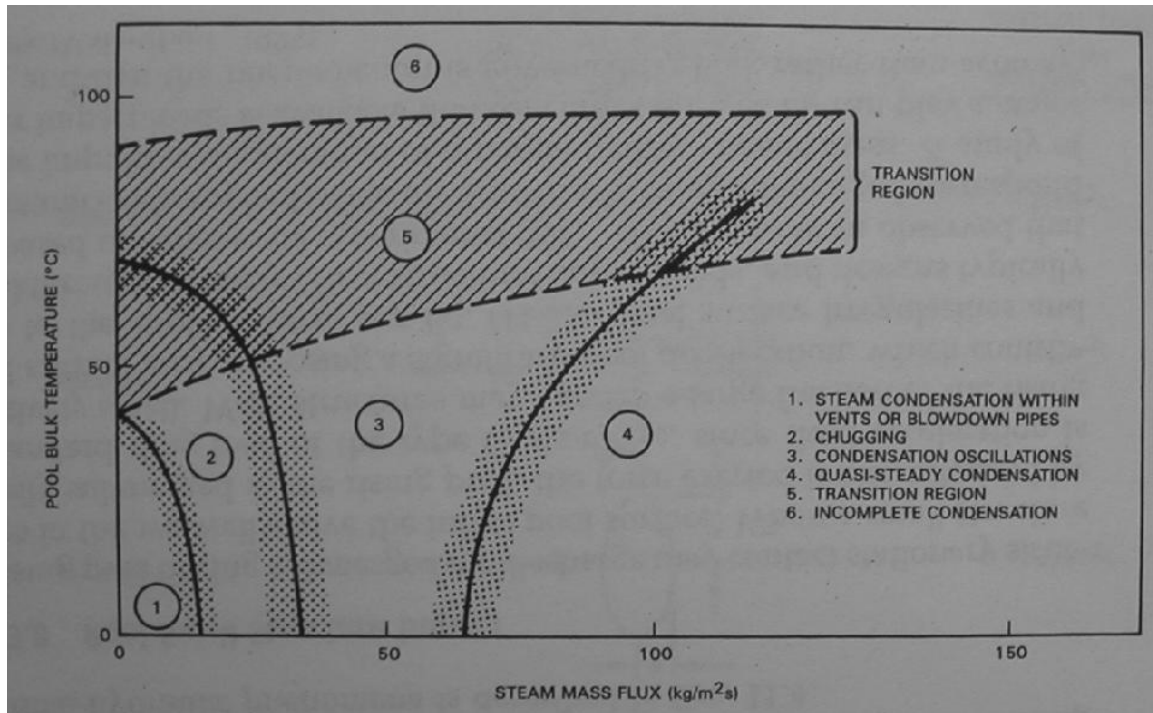


Figure 1. Condensation mode map when steam is blown into a pool of subcooled water (Lahey & Moody, 1993, page 582).

Steam bubbles periodically grow until condensation rate is high enough to make the whole bubble collapse, as steam is condensed into water and pressure inside the bubble instantaneously approaches zero. Water is sucked into the pipe, and driven out once again by steam pressure, repeating the cycle (see phases of the cycle below).

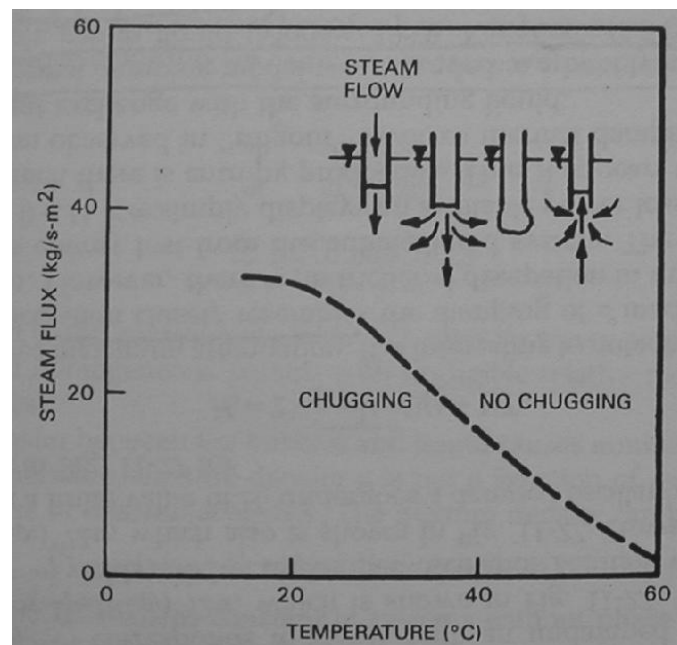


Figure 2. A sample chugging map and a diagram of the phases of a chugging cycle (Lahey & Moody, 1993, page 588).

Several chugging cycles may take place in one second. The oscillation causes pressure waves propagating through the water to pool walls. Chugging and condensation oscillations generally cause more severe pressure loads to the structures than the other condensation modes. The sample chugging pressure trace below shows an initial pressure peak of 4 kPa followed by a damped oscillation called ringout. In a real BWR case, pressure loads will be highest at the end of steam discharge, when there is no more air mixed with the steam, and thus very little damping of oscillations.

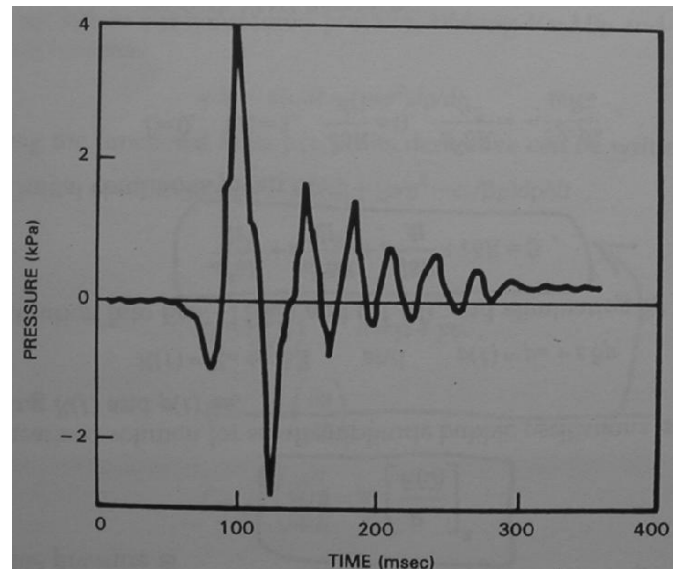


Figure 3. The pressure trace of a single chugging cycle (Lahey & Moody, 1993, page 588).

2.2 A Brief Literature Survey

Mainly for purposes of BWR plant design, chugging as well as other condensation modes have been studied both experimentally and theoretically since at least the 1970s.

Kerney et al. (1972) conducted experiments with a horizontally blowing steam injector, mainly with steam mass fluxes high enough to be in the steady condensation range. They also reported some theoretical studies concerning the condensation rate.

Wood et al. (1980) have performed a theoretical comparison study of methods to determine the pressure fields in a BWR suppression pool. They first calculate the exact solution by using Green's functions for an annular geometry and a point source. Then, they compare the results by the Method of Images (MOI) and by a finite difference technique with the exact solution and find very good agreement. They have got the pressure source for the MOI from a bubble dynamics model of a General Electric report.

Giencke (1981) solves the problem of wall loads in a realistic BWR suppression pool in three separate steps, based on potential flow. The first step is to calculate the pressure time history during the collapse of the steam bubble, for which Lord Rayleigh's bubble equations expanded for a finite pool with rigid walls are used, to arrive at a differential equation for the bubble radius. The second step is to calculate the spatial pressure distribution at any time instant from the potential due to a stationary source located in the center of the bubble. These steps can be expressed by writing the flow potential as $\phi = F(t) \psi(x, y, z)$, i.e. as the product of time-dependent and location-dependent parts (Giencke, 1981, page 177). Giencke arrives at

analytical expressions for (x, y, z) on pages 180-181. The third and final step of the analysis is the fluid-structure interaction.

Lahey & Moody (1993) have included in their BWR textbook a chapter on water expulsion and air / steam discharge loads, with dedicated text on chugging (pages 587-594). They arrive at a damped bubble radius oscillation (page 591), resembling the above pressure trace curve, by considering simultaneously the Rayleigh bubble equation and the energy balance equation of the bubble and choosing a suitable value for the heat transfer coefficient H_i . They also extend that model of thermal damping to a bubbly mixture that may contain air among the water.

Eerikäinen (1997) has written Fortran codes to calculate the pressure distribution in a pool of liquid according to potential theory. He derives the Poisson equation for pressure, as well as several alternatives for determining the pressure source, or more exactly, the total source strength, in Pa m, of the vector field $-\text{grad}(p)$. Eerikäinen also describes the formulation of the linear system of equations resulting from a spatially integrated form of the Poisson equation, the boundary conditions, and the successive over-relaxation (SOR) algorithm that solves the system. Finally, a user's guide to the Fortran codes (called SILA, from Simple Laplace) is included. By personal communication, Eerikäinen says that his method is preferable to the MOI.

Pättikangas et al. (2000) have simulated the water hammer in a pool due to steam bubble collapse by 2D CFD. They review the Rayleigh equations for the collapse of a spherical void bubble in an infinite pool of fluid (Lamb, 1975, page 122). Bubble radius (m), velocity of the bubble surface (m/s) and water mass sink (kg/s) for a 10 cm bubble are plotted for reference. Rayleigh equations are not applicable at the end of the collapse, as there the calculated velocity would approach infinity. The mass sink is found to have its maximum when bubble volume $V = V_0 / 4$.

Yadigaroglu & Lakehal (2003) review various future challenges in thermal hydraulics modeling, including the injection of steam/air mixtures from a downward facing vent into a water pool (particularly, in tests conducted in the PANDA facility in Switzerland). They propose a cascaded model, where Volume Of Fluid (VOF) simulations receive the necessary interfacial exchange laws for condensation heat and mass transfer from finer-level DNS (Direct Numerical Simulation) in real-time during the computation.

Youn et al. (2003) have conducted experiments, related to the KNGR (Korea Next Generation Reactor), where a horizontal vent discharges steam into a square pool of subcooled water. They investigate the DCC of steam in the chugging region and the induced pressure oscillations, and report experimental results, e.g. time histories of pressure and pressure pulse generation rates with various values of experimental parameters.

Laine & Puustinen (2005), among other POOLEX reports, describe the Lappeenranta University of Technology POOLEX condensation pool experiments, whose analysis and modeling this work strives for. In that report (POOLEX 4/2004) the experiments STB-13...STB-17 are described. Of those, STB-14 consists of eight separate steam blowdowns, which are located in the chugging region of the condensation mode map. The most important observations for the MOI purposes are the high-speed video (to see bubble dynamics) and the pressure measurements. Unfortunately, the highest speed of video used was only 220 fps (frames per second), yielding some ten frames during a typical bubble collapse. Furthermore, it seems that the only pressure measurement in pool water is one point at the bottom, with an error estimate of ± 5 kPa. More points would be needed to compare calculated pressure

distributions. The measurement error should preferably also be reduced, since the wall pressure loads (extra pressure due to chugging) are roughly in the same order of magnitude.

The basic dimensions of the POOLEX test rig are repeated here for easy reference:

- water level from 3.0 to 3.8 m from the center point of the bottom,
- inner diameter 2.4 m,
- height of the bottom cone 0.454 m,
- location of the blowdown pipe end: 1 m up from bottom, 0.3 m horizontally from the center z-axis.

Timperi et al. (2004) have studied the problem of pool wall loads by CFD simulations, FE analyses and one-directional FSI using Star-CD and ABAQUS. Correlations for the (maximum) bubble size and oscillation frequency are reviewed. A publicly available computer code (PELE-IC) is described that would calculate fluid pressure fields and structural responses using two-directional coupling. The Rayleigh equations for the collapse of a spherical void bubble in an infinite pool of fluid are reviewed as in Pättikangas et al. (2000).

Pättikangas et al. (2005) report studies that are a direct precursor of the present work. The MOI and the homogeneous two-phase CFD model are presented as alternative solution methods for the fluid pressure field problem (without structure considerations). Then, also a fluid-structure interaction (FSI) analysis of the pool is presented. The MOI section by Timo Narumo is carried further in this work.

2.3 Potential Flow

Potential flow is a hypothetical case of fluid flow that contains simplifications (irrotational flow, incompressible fluid) making it actually unphysical. However, many real physical flow situations can be approximately modeled as potential flow, depending on what details one is interested in. For easy reference, the basic assumptions of potential flow are briefly summarized here.

In potential flow, the fluid velocity vector field v is special in that it can be expressed as

$$v = \nabla \Phi$$

where Φ = fluid flow potential (scalar field).

It is also true in potential flow that

$$\nabla \cdot v = 0 \quad (\text{i.e. volume is conserved – no sources or sinks due to compressibility})$$

and

$$\nabla \times v = 0 \quad (\text{i.e. irrotational flow – no vortices}).$$

It is directly seen that Laplace's equation holds for the flow potential:

$$\nabla^2 \Phi = 0$$

From the momentum equation of frictionless flow it can, with little manipulation, be seen that in potential flow also the pressure as such satisfies Laplace's equation (Eerikäinen, 1997, p. 2). This is also shown, starting from the unsteady Bernoulli equation, by Lahey & Moody (1993, p. 574) for the time instants of minimum and maximum of bubble oscillations:

$$\nabla^2 p = 0$$

If there is a source of the pressure gradient in the domain of consideration, one gets instead the Poisson equation for pressure:

$$\nabla^2 p = -s_p$$

where $-s_p$ is the density of the source of the pressure gradient vector field. The physical unit of the source density is Pa m per cubic meter, or Pa/m².

It is obvious that the assumptions of potential flow cannot hold in a flow situation as violent as chugging. The flow is dynamically changing all the time, turbulence is present and even small amounts of air injected as a mixture with the steam appear as compressible bubbles in the pool water. However, calculations based on potential flow can probably be justified when the only significant output are the pressure loads on pool walls. For example, with a harmonically oscillating bubble, at the time instants of maximum pressure, all flow velocities equal zero (Eerikäinen, 1997, p. 4), which means that friction is not in effect at that time instant. Furthermore, as Narumo points out in Pättikangas et al. (2005), the velocity of the steam-water interface during bubble collapse is in the order of 10 m/s, which is smaller by a factor of 100 than the speed of sound in water, justifying the assumption on incompressibility.

2.4 Numerical Solution of Poisson Equation

With the assumptions of potential flow described above, the goal of finding pressures at pool walls reduces to solving the Poisson equation for pressure in the pool. The domain in the POOLEX condensation pool has two kinds of boundaries: the rigid (or assumed rigid) steel walls, and the free water surface of the open pool. They both have their specific boundary conditions for the pressure:

1. On the rigid walls, the pressure gradient in the direction of the wall normal must be zero ($\partial p / \partial n = 0$). The necessity of this condition can be seen from the momentum equation, observing that when fluid cannot flow through the wall and wall does not move, the flow velocity at the wall in the normal direction must be zero.
2. At an open pool's free surface, adjacent to atmospheric air pressure, the extra pressure due to chugging should be zero ($p = 0$). It remains somewhat questionable how the surface should be defined, as under the conditions of chugging the surface is not stationary. Note that also the atmospheric pressure and the hydrostatic pressure of pool water contribute to the total pressure in the pool.

The MOI considered in this work can be described as an indirect (or transform) method of solution. It is probably not the best choice in strict sense, because it introduces additional simplifying assumptions. Eerikäinen (1997) discusses the various other (more straight-forward) possibilities to solve this boundary value problem. It is similar to 3D heat conduction. The starting point could be the Poisson equation as such (terms written per volume) or preferably, as Eerikäinen suggests, some equivalent form with source integrated

over volume or pressure gradient integrated over bounding area. He proceeds by equating, for each grid cell, pressure gradient integrated over grid cell area with source integrated over grid cell volume. Then, the resulting linear set of equations is solved iteratively by a Successive Over-Relaxation (SOR) method in the SILA code.

Common to all solution methods, MOI or other, is the assumption of potential flow (giving the Poisson equation for pressure), independence of possible movements of walls or other structures, and the necessity to find the value of the source term.

2.5 Method of Images

The MOI is used e.g. in electrostatics and hydrodynamics. It is based on linearity and the uniqueness theorem for solutions to Laplace's equation. If two different arrangements of sources, sinks and zero potentials have their potentials satisfying Laplace's equation, then the potentials being equal on some closed surface implies that the potentials are equal everywhere. So it is possible to transform a particular arrangement into another one that is equivalent but easier to calculate. The assumptions and transformations of MOI have been listed in Pättikangas (2005, p.10), together with assumptions of potential flow, but let a few main points as well as the MOI formula be repeated here:

- It must be assumed that the pool is rectangular. This makes possible the mirroring about planar faces of the pool.
- The free water surface where pressure is zero can be transformed to a point sink, equal in magnitude to the real pressure source (steam bubble), located symmetrically above the surface over the source.
- The rigid walls where pressure normal gradient is zero can be transformed to point sources, equal in magnitude and sign to the real source, located symmetrically 'behind' the walls.

For the convergence of the method, it is necessary to expand the system of sources and sinks sufficiently in all directions. This is comparable to expanding the Green's function in terms of eigenfunctions in the exact solution Wood et al. (1980). There are several ways of doing the expansion, all leading to the same result but some converging faster than others. Wood et al. (1980) find best convergence with an expansion that is symmetric about the free water surface; see figure below.

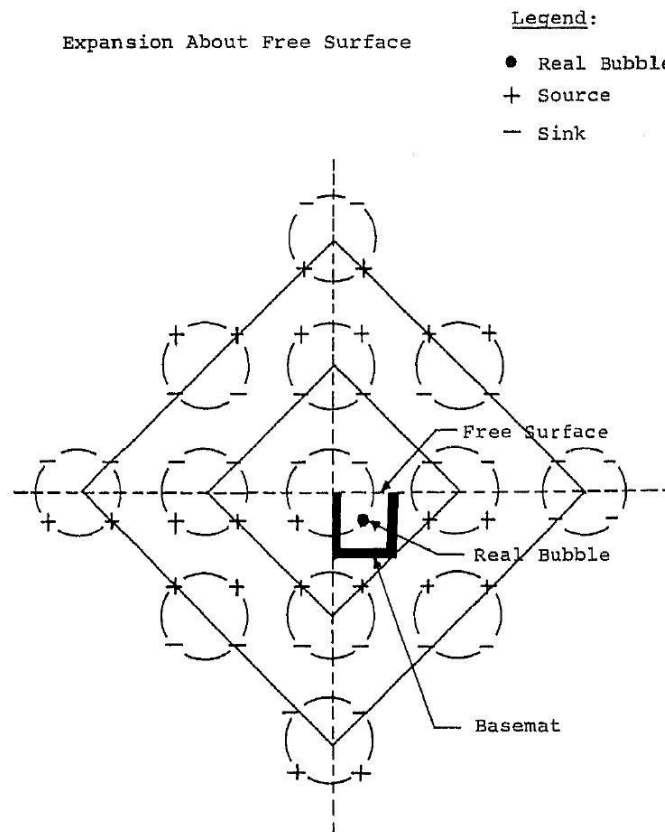


Figure 4. Schematic illustration of the Method of Images (Wood et al., 1980, p. 154). The bold-line object is the condensation pool. To achieve asymptotical convergence, an array of virtual sources and sinks is expanded to all directions from the real source. In this case, the array is symmetric about free water surface.

The MOI solution for the extra pressure caused by one point source can be written in the following simple form:

$$p(x, y, z) = S \sum_{i=1}^n \frac{\pm 1}{r_i} \quad \text{where}$$

- | | |
|--------------|---|
| $p(x, y, z)$ | = extra pressure at the point of interest (x, y, z) |
| S | = total source strength of the real pressure source (in Pa m) |
| n | = total number of sources and sinks (real source and all the virtual ones) |
| ± 1 | = +1 for a source, -1 for a sink |
| r_i | = distance from point source or sink i to the point of interest (x, y, z) |

2.6 The Fortran Code moi.f

From Tuunanen & Narumo (2004), a Fortran code called moi.f is available for calculating chugging pressures in a condensation pool by the MOI. The program calculates the pressure and its spatial partial derivatives at the points requested by user, but only for one instant of time in one run. It can handle multiple real sources (currently the maximum number is 110) and takes as input their co-ordinates and source strengths. Other input includes the extent of

expansion to virtual sources and sinks and dimensions of the pool, as well as pool shape parameters.

The `moi.f` code compiles and runs smoothly on a PC computer with Digital Visual Fortran. It is easy to plot pressure distributions from its output. `Moi.f` is not a big code, only appr. 1900 lines, but unfortunately there is no documentation to it. There are a handful of high-level comments by which it is fairly easy to follow the general flow of the calculation, but the details are not explained in any way, which makes any modification of the code substantially riskier than that of a well-documented code.

Another negative feature of the code is its relatively long running time. A typical calculation for about 3000 points (which is not much) takes some 8 min on a new 3 GHz computer, when reasonable convergence is required (35 reflections in each direction); and that is for only one instant of time. Eerikäinen (1997) reports having used 300 000 points in 1996 with his solution method. The slow running of `moi.f` might be due to using an expansion about the bottom of the pool, which makes MOI convergence slow.

An interesting feature of `moi.f` is its ability to calculate source strengths for multiple simultaneous sources, when their bubble radii and pressures are given in the input, presumably at the instant of maximum bubble radius. When steam is blown down from multiple vents, it is not possible to perform a straight-forward superposition of solutions (as one might expect from linearity), because each pressure source is readily affected by the pressures caused by the other ones Eerikäinen (1997, p. 4). It seems that the `moi.f` code solves all the simultaneous source strengths iteratively from a linear set of equations containing bubble radii and pressures.

2.7 Determination of the Pressure Source

The main left-open question in the previous work was how to determine the pressure source. It seems that at that time the determination was done largely on an ad-hoc basis, described as follows in Pättikangas et al. (2005): “The point source strength is determined as: the extra pressure due to chugging at the locations of maximum estimated bubble radius is assumed to be equal to the hydrostatic head of water at that depth. This is assumed to be the scale for local pressure when the bubble has just collapsed and the water shock wave following the rarefaction wave has appeared.”

2.7.1 The Method of Wood et al. (1980)

Wood et al. (1980, p. 155) give a simple formula, derived from the equations of mass and momentum conservation, for the pressure source to be used for MOI:

$$S = R_B (P_B - P_\infty) + \frac{\rho_L \left| \dot{R}_B \right| \dot{R}_B}{2g_c} \quad \text{where}$$

R_B = bubble radius
 P_B = bubble pressure
 P_∞ = reference pressure

Wood et al. (1980) refer to ‘both pressure and acceleration loads’, and there seem to be two separate terms in the source strength formula. The physical unit of the first term is obviously Pa m, as required, but unfortunately, the second term is somewhat more questionable.

2.7.2 Solution of Pressure Source by moi.f

The Fortran code moi.f was already introduced above. It has subroutines for solving source strengths of multiple simultaneous sources, when their bubble radii and pressures are given in the input. The solution proceeds iteratively from a linear set of equations, formed by the subroutine ‘matrix’. Unfortunately, as there are no comments, it was not possible within this work to take the extra effort needed to ‘reverse-engineer’ the theoretical background of the solution.

2.7.3 Pressure Source from Second Time Derivative of Bubble Volume

Eerikäinen (1997, p. 3) has, starting from the surface integral of the pressure gradient, derived a formula for the pressure source (Pa m):

$$S_p = \rho_L \frac{d\dot{V}_B}{dt} \quad \text{where}$$

$$\begin{aligned} \rho_L &= \text{density of water (kg/m}^3\text{)} \\ V_B &= \text{volume of steam bubble (m}^3\text{)} \end{aligned}$$

It is seen that the magnitude of the source is proportional to the second time derivative of the bubble volume, or ‘volumetric acceleration’. Thus, steady expansion (or collapse) of a bubble should not cause a pressure wave. It must be noted here that the change of volume is the same for any domain enclosing the bubble, since water is incompressible.

2.7.4 Pressure Source from Maximum Rate of Change of Bubble Volume

Another formula for pressure source maximum value, derived by Eerikäinen (1997, p. 4) from the assumption of a harmonically oscillating bubble, involves the maximum rate of change of bubble volume:

$$S_{\max} = -\rho_L \omega \dot{V}_{\max} \quad \text{where}$$

$$\begin{aligned} \rho_L &= \text{density of water (kg/m}^3\text{)} \\ \omega &= 2\pi f = \text{angular speed of the harmonic oscillation (1/s)} \\ V &= \text{volume of steam bubble (m}^3\text{)} \end{aligned}$$

So here the maximum value of the pressure source is proportional to the maximum rate of change of the bubble volume.

2.7.5 Theoretical Expressions for Bubble Volume

To be able to use the above formulas for pressure source, one needs information from bubble dynamics: the radius of the collapsing bubble as a function of time. From the radius, one gets all the necessary velocities, volumes etc.

The classical formulas for collapse of a steam bubble in an infinite pool of water are those derived by Lord Rayleigh. They are given and plotted e.g. in Timperi et al. (2004, p. 15), and are not repeated here. However, let it be mentioned that the maximum value of mass sink for water (kg/s) was found to be when $V = V_0 / 4$, in other words, the bubble has collapsed to one fourth of its original volume.

In a practical situation, the finite size of the pool may slow down the collapse a little bit, as it is not as straight-forward for the water to flow to fill the space left by steam. Giencke (1981) uses an extension of the equations for a finite pool. Also, in practice there is the blowdown pipe, filled with steam, connected with the bubble, and the collapse water will start moving upwards the pipe for some time in chugging.

In their section on chugging, Lahey & Moody (1993, p. 589) consider simultaneously the Rayleigh bubble equation and the energy balance equation of the bubble. They derive a pair of ordinary differential equations that lead to an oscillating bubble, whose radius changes in similar fashion as the pressure trace of a single chug shown above. From the equations, bubble radius and pressure can be solved as a function of time. It remains to choose a suitable value for the heat transfer coefficient H_i . That defines the DCC heat transfer from steam to water. Obviously, it is not easy to know the correct value of H_i . Below the lowest (damping) curve of bubble radius is one that they got with a H_i giving maximum possible damping. There are even some results derived by Lahey & Moody (1993, pp. 590 – 594) for bubbly mixtures containing air in the pool water.

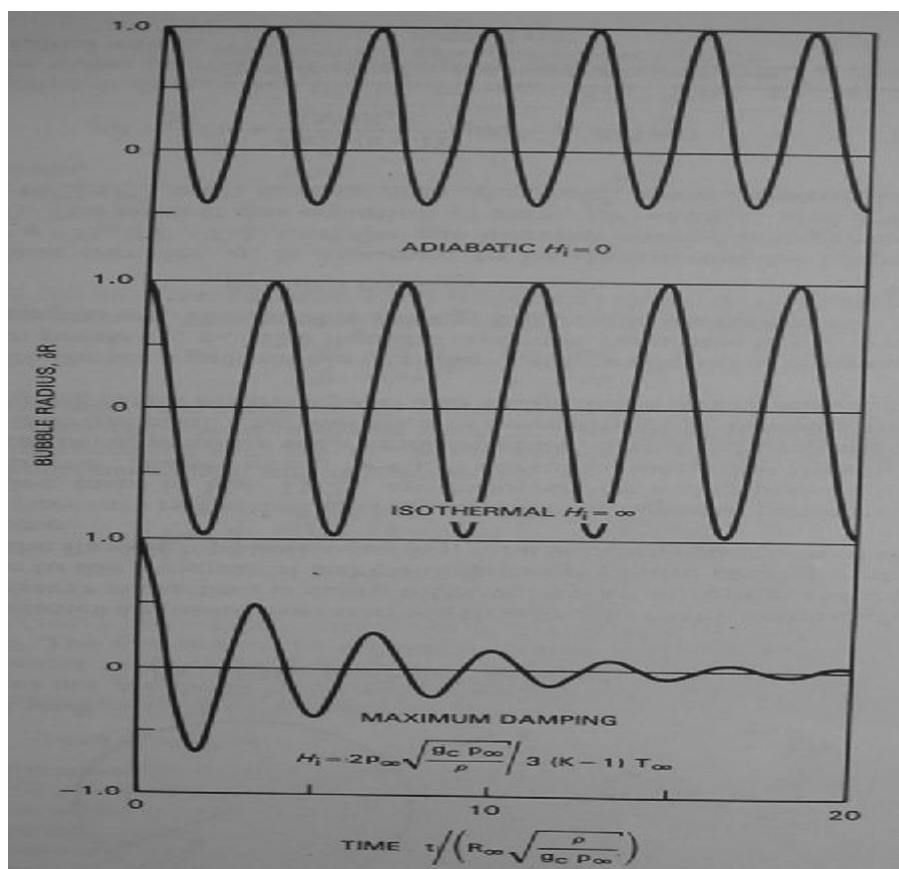


Figure 5. Sample results from a model of damping oscillations in chugging. The three cases were calculated with three different values of the condensation heat transfer coefficient (Lahey & Moody, 1993, p. 591).

2.7.6 Experimental Determination of Bubble Volume

It would be feasible (though requiring a lot of manual work) to determine the radius of the steam bubble from high-speed video observations of the POOLEX experiments. With enough radius values per time unit, one would get also the numerically calculated values of the first and second time derivatives of the radius, as well as all the similar information of bubble volume. This information could then be used to test the various methods of determining the pressure source, as well as methods of calculating the pressure loads from the pressure source, with well-known data from a certain experiment. Finding the working formulas and methods would then contribute to calculating any new case, like steam blows in a real power plant. The problem with the POOLEX experiments conducted so far is that the fps (frames per second) speeds of video were not high enough. Only some 200 fps was used, yielding some ten frames during a typical bubble collapse. The camera is, however, capable of 10000 fps. Suitable experiments, featuring the chugging phenomenon, are e.g. STB-14, STB-23 and STB-24. Of these, STB-14 was reported in Laine & Puustinen (2004); the other two were not yet reported, as they are quite recent.

2.7.7 Pressure Source from the Divergence Theorem

A simple and innovative way of determining the pressure source from experimental data, mentioned by Eerikäinen (1997, p. 3), is based on the surface integral of the pressure gradient. Integrating the pressure gradient over any closed surface containing the source will yield the total strength of the pressure source in Pa m. It is easiest to use the perimeter (or hull) of the water mass in the pool. Then, the integral over rigid walls is zero, because there the pressure gradient is necessarily zero. It remains to multiply the area of the pool with the pressure gradient near free water surface. The latter can be assumed almost constant, if the pool is high (compared with its width) and the source is deep in water. Some difficulties might be caused by the blowdown pipe, which makes it difficult to enclose the source inside a closed surface, as required in the divergence theorem. Practical difficulty for the time being is that there are no pressure measurements from the top of the POOLEX pool, as these were not considered useful.

2.8 Suggestions for Pressure Source Studies

As there are various potential ways of determining the pressure source, it would be useful to know its correct value. One method of approaching would be to do some ‘reverse’ calculations, i.e. find the value of pressure source that will produce the measured pressure distributions, over space and time, as closely as possible. This is technically easy to do by computer. Obviously, there is no unique definition of ‘closely’ in this kind of setting, but some common error criterion might be used. The practical problem is that there are not enough pressure measurement points in the pool water. Comparing just one point may falsify the results too much.

Once this reverse calculation were done, it would give some new perspective to comparing the formulas for pressure source. Do they give values close to each other, and do at least some of them give a value close to the appearing-correct one?

3 Homogeneous Two-phase Model for CFD Calculations

In this section a homogeneous two-phase fluid model for water and steam has been implemented in Fluent environment. The homogeneous two-phase fluid model considered here is a straightforward adaptation of the model implemented in the APROS 1D code. The work presented here is an extension to work made earlier in this project using Star-CD environment.

The Star-CD implementation was able to simulate steady-state cases. The transient simulation however failed to converge. The divergence was supposed to result from the lack of SIMPLE type iteration procedure in transient calculations. In the new Fluent version 6.2.16 the SIMPLE method can be used and the new code feature makes possible the compressibility modeling by means of the speed of sound for the fluid. The latter feature is fundamental in implementing the homogeneous two-phase fluid model.

3.1 Outline of the Implementation

In very early stage of model testing it was realized that the turbulence models (k-epsilon, k-omega, Spalart-Almaras) cause convergence problems that cannot be solved in the limited time frame. Therefore, only laminar flow was considered.

3.1.1 Pressure-Flow Solution

The standard momentum and mass equations have been used without any extra source terms.

$$\frac{\partial \rho}{\partial t} + \frac{\partial \rho u_j}{\partial x_j} = 0 \quad (1)$$

$$\frac{\partial \rho u_i}{\partial t} + \frac{\partial \rho u_j u_i}{\partial x_j} = -\frac{\partial p}{\partial x_i} + s_i \quad (2)$$

The homogeneous water-steam mixture is described by user-defined functions for density, viscosity and speed of sound. The effective viscosity used is 10 times larger than the real molecular viscosity in order to have some turbulence effects. For more detailed description of pressure-flow solution see Pättikangas et al. (2005).

3.1.2 Heat Transfer Solution

For reasons described earlier in Pättikangas et al. (2005) the standard energy/enthalpy equation has been replaced by a user defined scalar transport equation for the mixture enthalpy.

$$\frac{\partial \rho h}{\partial t} + \frac{\partial (\rho u_j h - F_{h,j})}{\partial x_j} = \frac{\partial p}{\partial t} \quad (3)$$

$$F_{h,j} = \frac{k}{c_{eff}} \frac{\partial h}{\partial x_j} + \frac{\mu_t}{Pr} \frac{\partial h}{\partial x_j} \quad (4)$$

$$c_{eff} = Xc_{p,steam} + (1 - X) \cdot c_{p,water} , \quad (5)$$

where X is steam mass fraction.

Because the standard energy/enthalpy equation for fluid is not in use one cannot use the wall heat conduction model provided by the CFD code. Here a simple 1D solid heat conduction model has been connected to the user defined energy equation. The fluid-solid heat transfer model has been described in detail in Pättikangas et al. (2005).

3.2 Test Case

The test case consists of a vessel filled with cold water. Steam enters the vessel in a vertical pipe. The system represents the POOLEX test facility and has been depicted in Fig. 6. The following parameters were used:

- Water: temperature 10 °C, enthalpy 40000 J/kg
- Steam: temperature 162 °C (T_{sat} 133 °C at 1.3 bar), enthalpy 2.8×10^6 J/kg
- Steam flow 0.4 kg/s

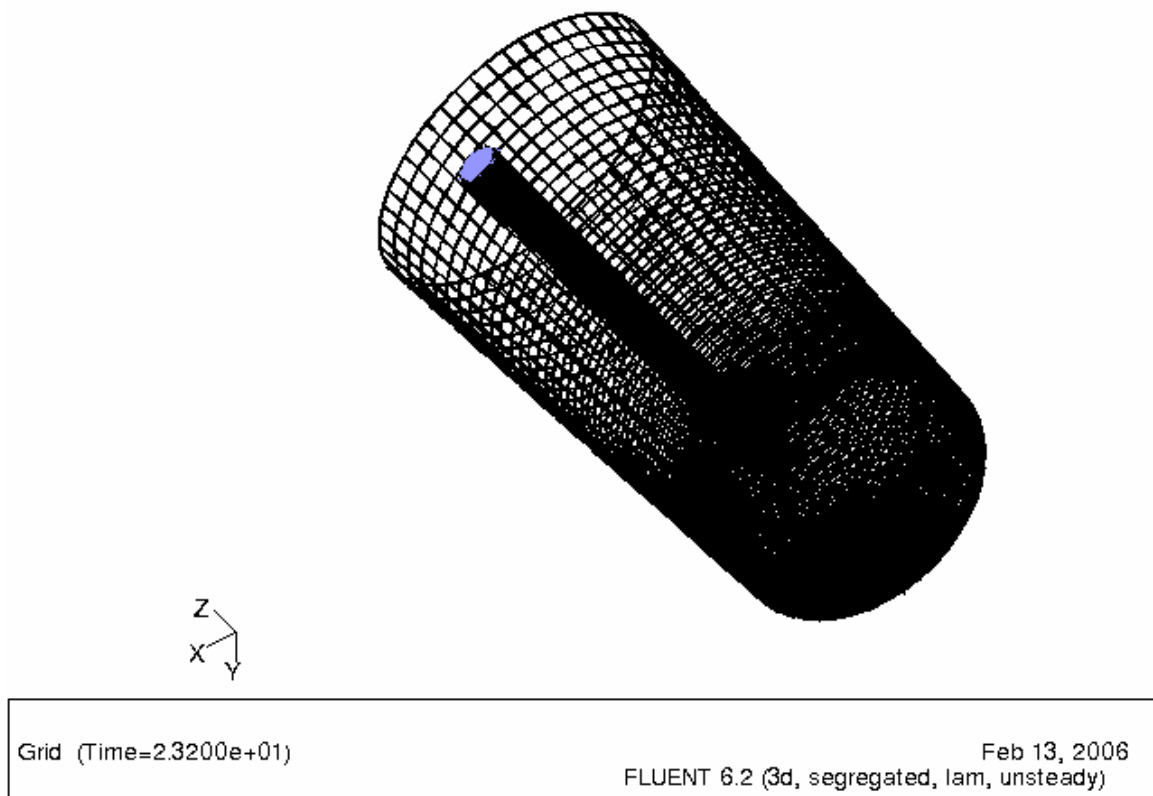


Figure 6. Grid layout.

3.3 Test Calculations

In transient simulations the problems begin when the first phase changes take place resulting in divergence. A typical steam void fraction field at the moment of divergence has been

depicted in Fig. 7. The pressure-enthalpy behaviour of an individual cell during iteration has been depicted in Fig. 8.

After the transition from pure water to two-phase region the pressure and enthalpy remain bounded but enthalpy changes are positive making the solution to drift away from the physical solution near the water / two-phase boundary. Finally the enthalpy corrections start to oscillate leading to divergence. The divergence seems to be a problem only in the two-phase region. Pure water and pure steam simulations do converge.

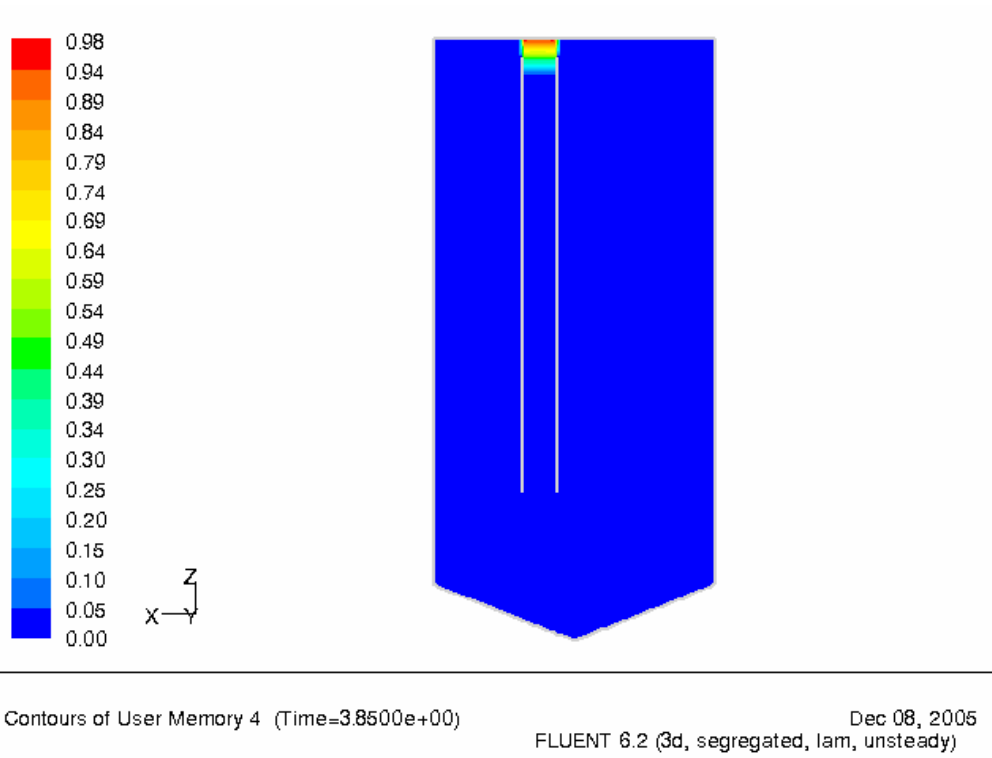


Figure 7. Void fraction.

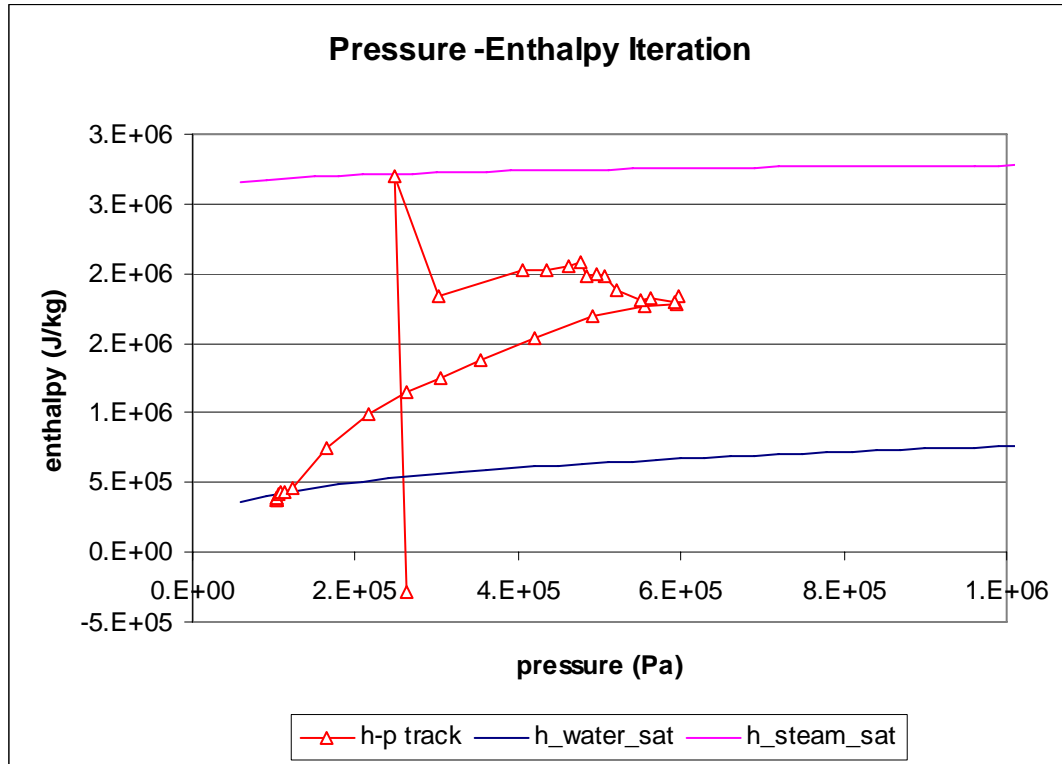


Figure 8. Diverging iteration.

3.3.1 An Explanation for Divergence

The enthalpy equation has been examined in a single cell case. The enthalpy equation for a cell in the pipe inlet has been integrated over the cell volume. The diffusive terms and horizontal flow effects have been ignored. Here pressure and velocity are known because they have been solved already at the first stage in SIMPLE iteration.

$$Energy^{new} = energy^{old} + energy_{in} - energy_{out} + pressure_effects \quad (6)$$

$$Energy^{new} = \rho^{new} h^{new} \cdot volume \quad (7)$$

$$Energy_{out} = \rho^{new} h^{new} \cdot u_{out} \cdot area \cdot \Delta t$$

This leads to an equation for the new energy density

$$\rho^{new} h^{new} = \frac{energy^{old} + energy_{in} + pressure_effects}{volume + u_{out} \cdot area \cdot \Delta t} \quad (9)$$

In the Fluent enthalpy equation solution the density is determined by the pressure and enthalpy from previous iteration. In Fig. 9 the energy density as function of enthalpy has been depicted. In two-phase region the energy density decreases as enthalpy increases unlike the linearized case that is solved in the Fluent solution system. That is if the mixture enthalpy solved at previous iteration is too high so that the corresponding density is too low then at the next iteration even higher value of mixture enthalpy is obtained. This true energy density versus linearized energy density problem does not exist in the pure water region and in the

pure steam region the problem is of minor importance. The problem is related to the fact that in the mixture enthalpy equation the density is treated as constant. In principle one could add the density enthalpy dependence by using density in form

$$\rho^{new} = \rho(p, h) \approx \rho(p, h_k) + \frac{\partial \rho}{\partial h} (h - h_k),$$

where subscript k refers to previous iteration.

Applying this approximation in the time derivative term of the enthalpy equation the following additional source term is obtained to the right hand side of the equation

$$S'(h) = -\frac{1}{\Delta t} \frac{\partial \rho}{\partial h} (h - h_k) h, \quad S'(h_k) = 0$$

$$\frac{\partial S'}{\partial h} = -\frac{1}{\Delta t} \frac{\partial \rho}{\partial h} (2h - h_k), \quad \frac{\partial S'}{\partial h} \Big|_{h=h_k} > 0$$

Unfortunately the derivative term would not be taken in the matrix solution because the term would decrease the diagonal element of the matrix.

Several ad hoc attempts to circumvent the problem with energy density in the two-phase region have been tried. Two of them will be described in some detail in the following.

3.3.1.1 Change of Enthalpy Variable

$$h \equiv h - h_{ref} + h_{ref} \tag{10}$$

$$h = h_e + h_{ref}, \text{ where } h_e = h - h_{ref}$$

Substituting h an equation for the enthalpy h_e is obtained. The left hand side is similar to mixture enthalpy Eq. 3. There is an additional term on the right hand side

$$S'' = -\left[\frac{\partial \rho h_{ref}}{\partial t} + \nabla \cdot (\rho \bar{u} h_{ref}) \right]. \tag{11}$$

After some manipulation S'' can be expressed as function of pressure

$$S'' = -\rho \frac{\partial h_{ref}}{\partial p} \left(\frac{\partial p}{\partial t} + \bar{u} \cdot \nabla p \right). \tag{12}$$

Experiments were made using $h_{ref} = h_{sat_water}$ and $h_{ref} = h_{sat_steam}$. The energy density function in these cases looked more promising (Fig. 10) though the enthalpy is now negative in most parts of the system. In both cases the simulation ended in divergence. The pressure transient of an unsuccessful simulation has been depicted in Fig. 11.

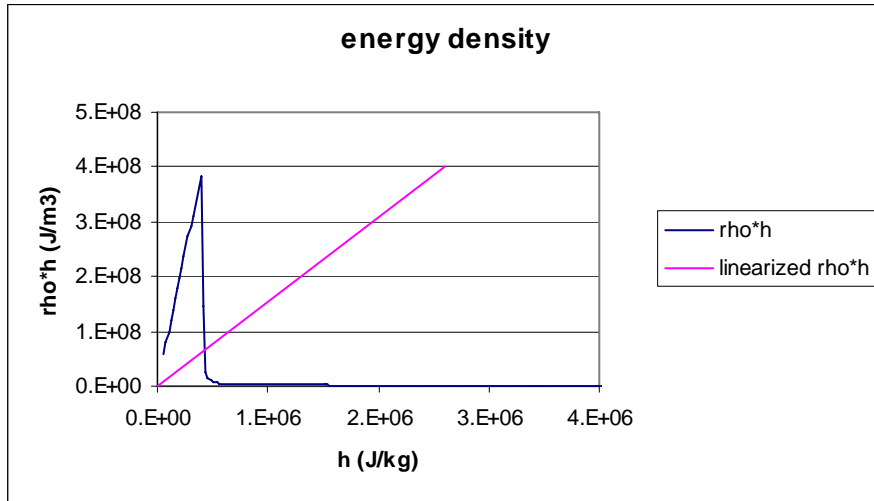


Figure 9. Energy density as a function of mixture enthalpy at 1 bar pressure. Water saturation enthalpy is 4.4×10^5 J/kg and steam saturation enthalpy is 2.7×10^6 J/kg.

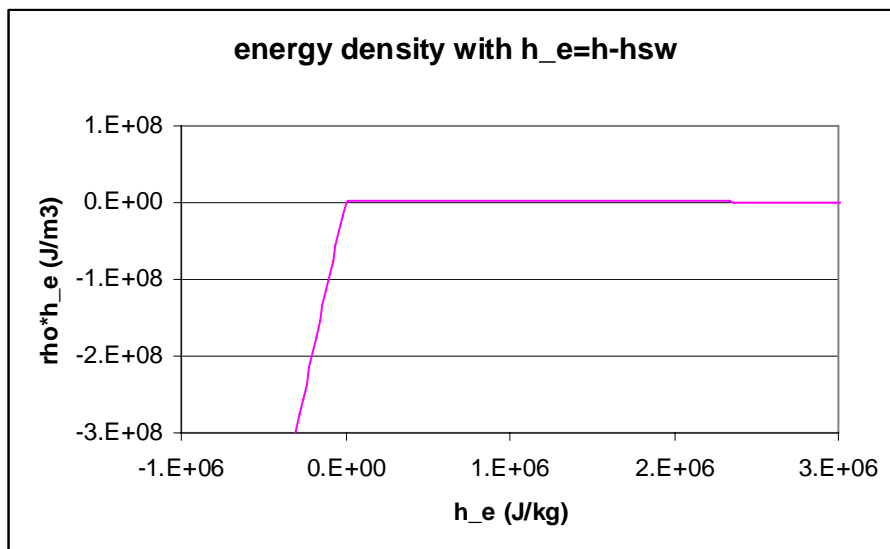


Figure 10. Energy density using effective enthalpy $h_e = h_{mix} - h_{sw}$.

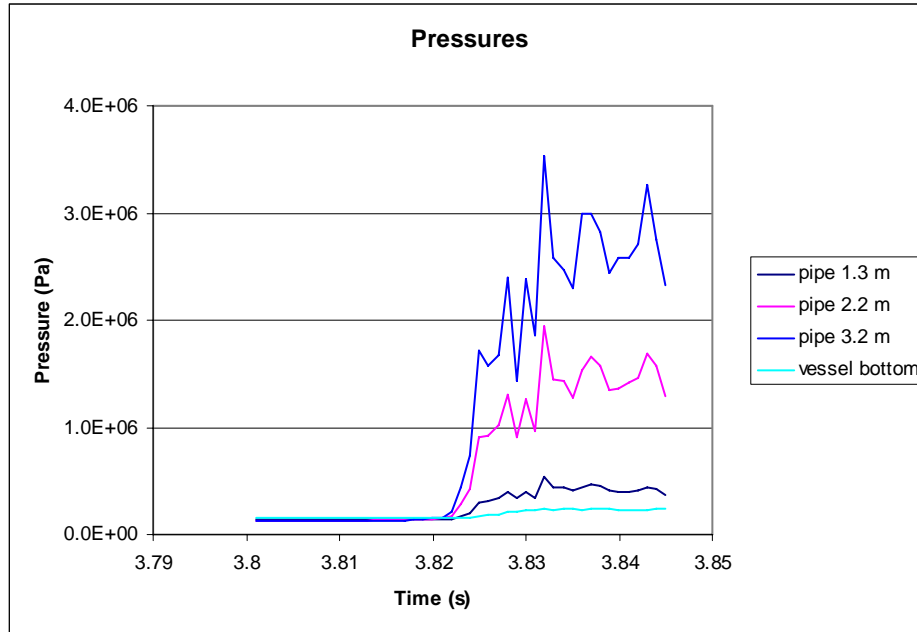


Figure 11. Pressure transient.

3.3.1.2 Energy Density Solution

Because the linearized energy density solution fails in the two-phase region it was tried to improve solution by solving the nonlinear energy density equation for each cell.

$$\rho(p, h)h = ene_dens \quad (13)$$

where $ene_dens = \rho(p_k, h_k)h_{k+1}$

Here ene_dens represents the energy density of the Fluent solution. The idea is to have a better density estimate for the next iteration. In this experiment the corrected enthalpy satisfies the energy density relation but not the flow equation. All of the test calculations failed.

4 Coupled CFD and Structural Analyses

In the following, fluid-structure interaction simulations with the MpCCI and ES-FSI codes are presented. The Fluent 6.2 CFD code (Anon., 2005a) is coupled with the ABAQUS 6.5 structural analysis code (ABAQUS, 2004) by using MpCCI 3.0 (MpCCI, 2005). ES-FSI is used for coupling the Star-CD 3.15 CFD code (Anon., 2001) with ABAQUS.

With both coupling methods, chosen POOLEX experiments with the DN 200 blowdown pipe were modelled. The CFD meshes used in the simulations were very similar to the one used originally by Pättikangas and Pokela (2003). The main difference is the larger diameter of the blowdown pipe, namely 200 mm, used in the present work. In addition, the structural model of the pool is nearly identical to the one presented by Timperi et al. (2004). The number of grid cells in the CFD meshes was about 80 000 and the number of elements in the structural model was 6706. The mesh used in the simulations with Star-CD and the structural model are shown in Fig. 12.

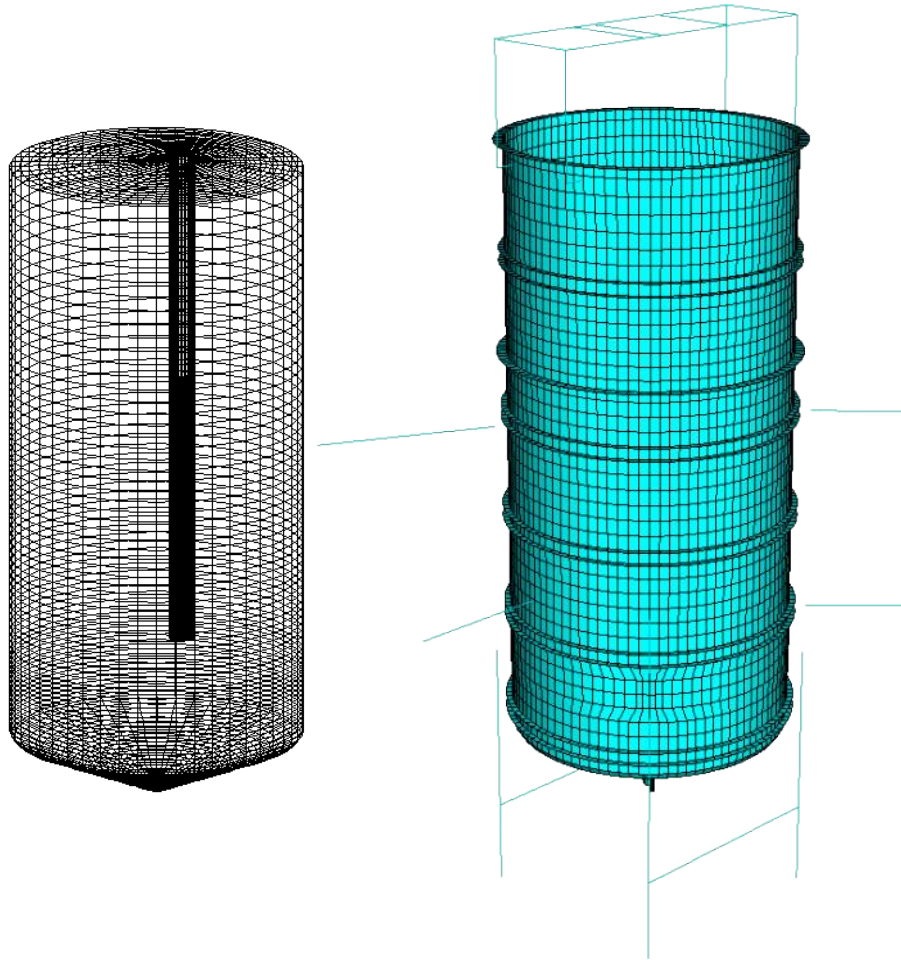


Figure 12. Surface mesh of the CFD model used in the simulations with Star-CD and the structural model of the pool.

4.1 Fluid-structure calculations with Fluent and ABAQUS

In this section, the fluid-structure interaction calculations performed with Fluent and ABAQUS are described. The new MpCCI version 3.0 code was used for coupling the flow and structural analysis. In one-directional coupling, MpCCI transfers the load from the flow simulation to the structural analysis. In two-directional coupling, the new positions of the wall nodes are transferred back from structural analysis to flow simulation. In both data transfers, MpCCI performs interpolation between different meshes of the two codes. In earlier work, an in-house tool written on top of earlier versions of MpCCI has been used (Pättikangas and Pokela, 2003). The present version of MpCCI with graphical user interface makes the in-house tools obsolete.

We first describe briefly a simulation of an academic test case with two-directional coupling: a box with flexible walls. Then the attempts to perform simulations with two-directional coupling for the POOLEX experiment are briefly discussed. Finally, simulations with one-directional coupling for the POOLEX experiment are described, where the new compressible Volume Of Fluid (VOF) model of Fluent 6.2 was used.

4.1.1 Simple Test Case: Box with Flexible Walls

The two-directional coupling of Fluent and ABAQUS was first studied by using as a test case a small box with dimensions $10 \times 10 \times 20 \text{ cm}^3$. The box is initially filled with air which is modeled as an ideal gas. The relative static pressure is initially zero and the flow velocity of air is zero. The box is open at one end, both the inlet frame and outlet frame of the box are rigidly attached (see Fig. 13).

The result of the test simulation is summarized in Fig. 13. At time $t = 0$, the pressure at the box inlet is increased by 0.5 bar, and air flows into the box with a velocity larger than 100 m/s. The pressure in the box is increased and achieves a maximum value of about 1.5 bars at bottom of the box within 1.8 ms. In Fig. 13, the flexible box calculated by ABAQUS is plotted with non-scaled deformations obtained directly from Fluent. Then pressure continues oscillating in the box with decreasing amplitude and with a period of 2 ... 3 ms, see Fig. 14.

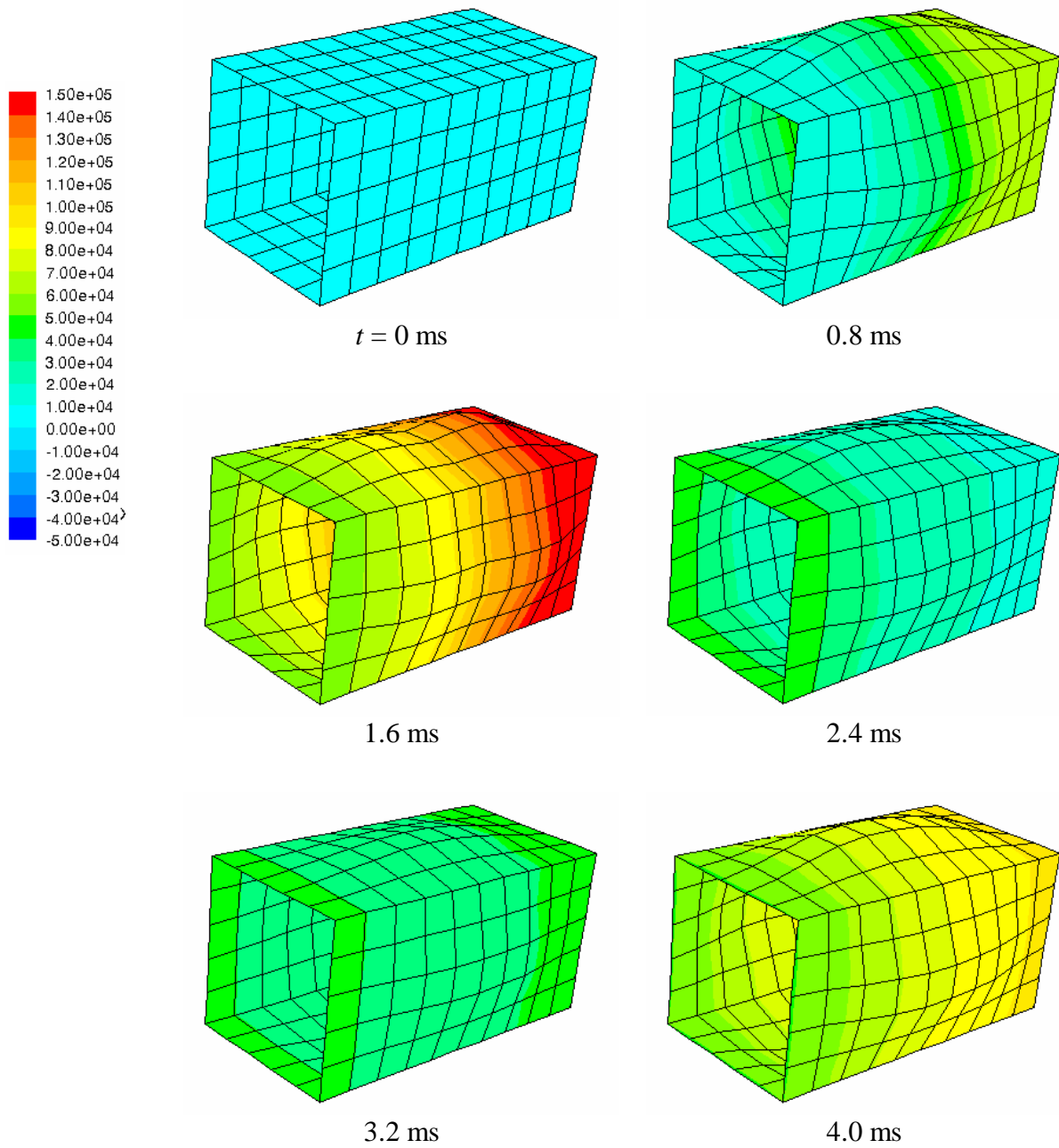


Figure 13. Static relative pressure on the wall of the flexible box. The deformation of the box is shown in actual scale.

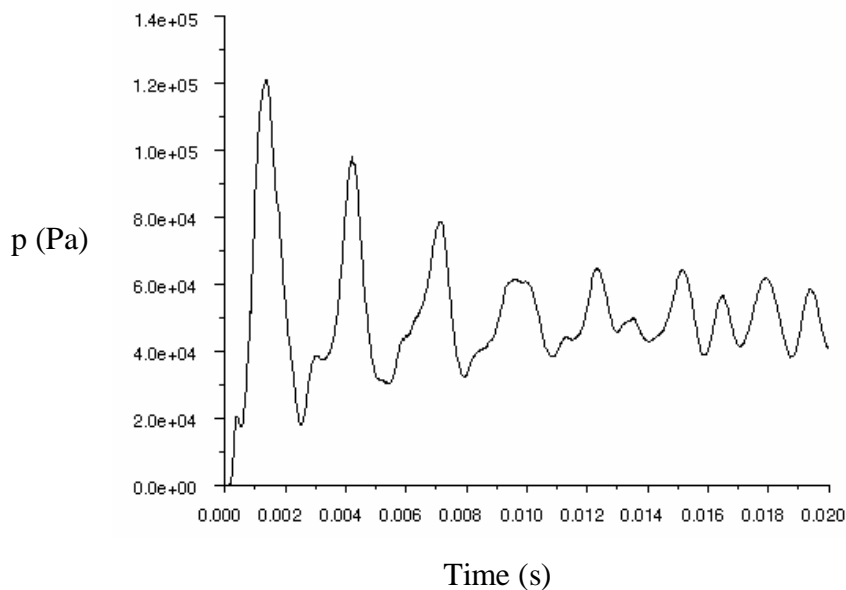


Figure 14. Relative static pressure at the center of the simple test box.

4.1.2 Water pool: Stability Issues in Two-directional Coupling

MpCCI 3.0 has two alternatives for performing the coupling of the codes: parallel and serial coupling. The serial coupling is more robust of these two. In the serial coupling scheme, ABAQUS first performs a time step without any load. Second, Fluent performs a time step and calculates the first pressure load, which is transferred to ABAQUS. Third, ABAQUS performs a time step using the pressure load calculated by Fluent and transfers the new node positions to Fluent. Then, Fluent performs a new time step by using the coupling wall geometry obtained from ABAQUS, and the cycle is repeated. In all the Fluent simulations, the serial coupling scheme was used.

In all performed test simulations for the water pool, both Fluent and ABAQUS used implicit time integration. The overall coupling cycle of the codes is, however, explicit. In performing implicit time integration, iteration between Fluent and ABAQUS in performing the time step would be necessary. However, such a coupling scheme is not available in MpCCI 3.0 as such.

The simulations of the POOLEX pool with two-directional coupling were found to become numerically unstable, when the amount of water was increased in the pool. Numerous attempts were performed in order to overcome the instability, but with no positive result. An example of slow numerical instability is shown in Fig. 15, where an attempt to calculate the stationary state of the pool was performed. An oscillation in the pressure starts gradually at time $t = 1.2$ s leading to divergence at time $t = 1.40$ s. When the amount of water or density of water is decreased by a factor of two, the calculation is numerically stable. This method is not, however, useful for practical purposes.

In the following, we only present results obtained with one-directional coupling for the POOLEX experiment.

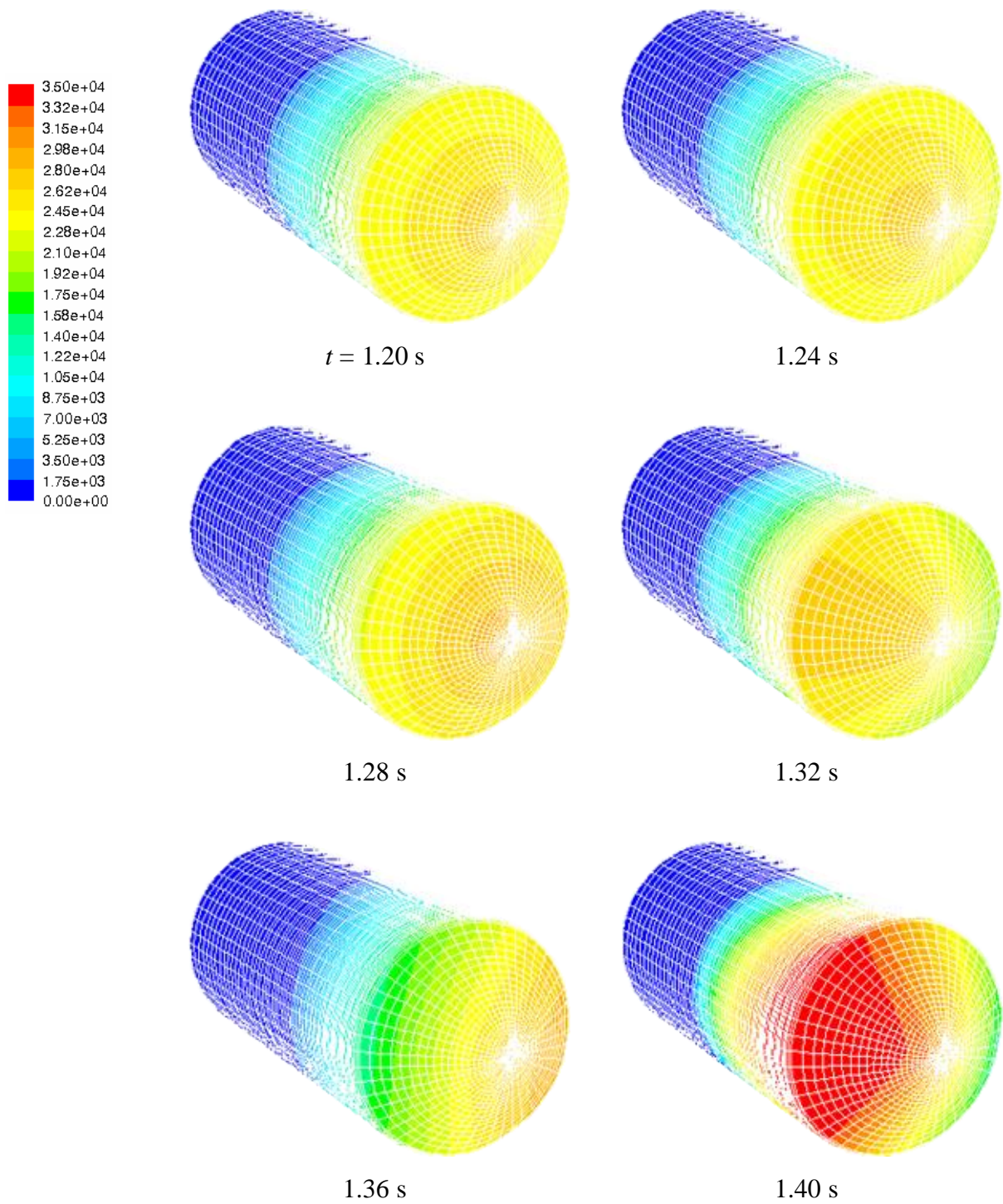


Figure 15. Static absolute pressure (Pa) on the pool wall during developing numerical instability when two-directional coupling is used.

4.1.3 Water Pool Simulation with One-directional Coupling

Since calculation of the water pool with two-directional fluid-structure interaction turned out to be unstable, MpCCI 3.0 was tested in calculation of the water pool with one-directional coupling. As a test case, blowdown of air was chosen which was simulated by using two different VOF models of Fluent. First, simulation was performed with the incompressible VOF model which has been used in previous calculations for the POOLEX experiment. In the incompressible VOF model, air is also treated as incompressible, which is not a very satisfactory approximation. Second, the new compressible VOF model of Fluent 6.2.16 was tested, where air was treated as an ideal gas but water was assumed incompressible.

When one-directional coupling is used with MpCCI 3.0, the Fluent and ABAQUS simulations are performed simultaneously. In the beginning of the simulation ($t = 0$), the load of the water starts affecting the pool structures and the pool starts oscillating. At time $t = 0.5$ s, the oscillation of the pool structures has damped and blowdown of air starts.

During the blowdown, constant mass flow boundary condition is used at the pipe inlet, where the mass flow rate is 0.25 kg/s. This corresponds to a mass flux of 8 kg/m²s used in the steam blowdown experiment STB-14-6, where the temperature of the pool was about 60°C. This experiment was in the transition region of the diagram in Fig. 1 (Laine and Puustinen, 2004). Since the pipe inner diameter is 200 mm, the corresponding flow velocity is 6 m/s, if the air density is 1.5 kg/m³. The present simulations were performed with laminar flow model.

4.1.3.1 Simulation with Incompressible VOF Model

The initial phase of the blowdown of air with the incompressible VOF model is shown in Fig. 16. When the blowdown of air starts at $t = 0.538$ s, air starts penetrating into the pipe and water is expelled from the pipe at time $t = 0.85$ s. The accelerated water plug hits the pool bottom followed by a jet of air. The flow velocity of air and water at the time of pipe opening was 6.6 m/s. At time $t = 1.0$ s, the first bubble is formed at the pipe outlet. Later it is detached and rises towards the pool surface. Then formation of a new bubble starts at the pipe outlet.

In the incompressible simulation, a spurious pressure peak occurs at time $t = 0.538$ s, immediately after the blowdown starts. This short pressure peak is a numerical artifact caused by the fully incompressible VOF model. This pressure peak can be avoided by using pressure boundary condition at the pipe inlet as was done in earlier studies on blowdown of air into water pool (Pättikangas and Pokela, 2003). In the present simulation, the effect of this pressure peak is damped before the loading caused by the water plug after $t = 0.8$ s becomes visible.

The pressure load at the pool bottom is illustrated in Fig. 17. The pressure load on the pool bottom reaches its maximum value at time $t = 0.90$ s, when the water plug hits the pool bottom. Some rapid pressure oscillations are also seen at $t = 1.0$ s, when the formation of the first bubble starts, and at $t = 1.15$ s, when water hits back to the pipe outlet.

In Fig. 18, von Mises stress is shown on the inner wall of the pool. In the incompressible simulation, the water level in the pool was 3.2 m. The corresponding steady state value of von Mises stress was about 76 MPa at the rounding of the pool bottom. Maximum stress value of 80 MPa occurs at $t = 1.0$ s, somewhat after the maximum loading.

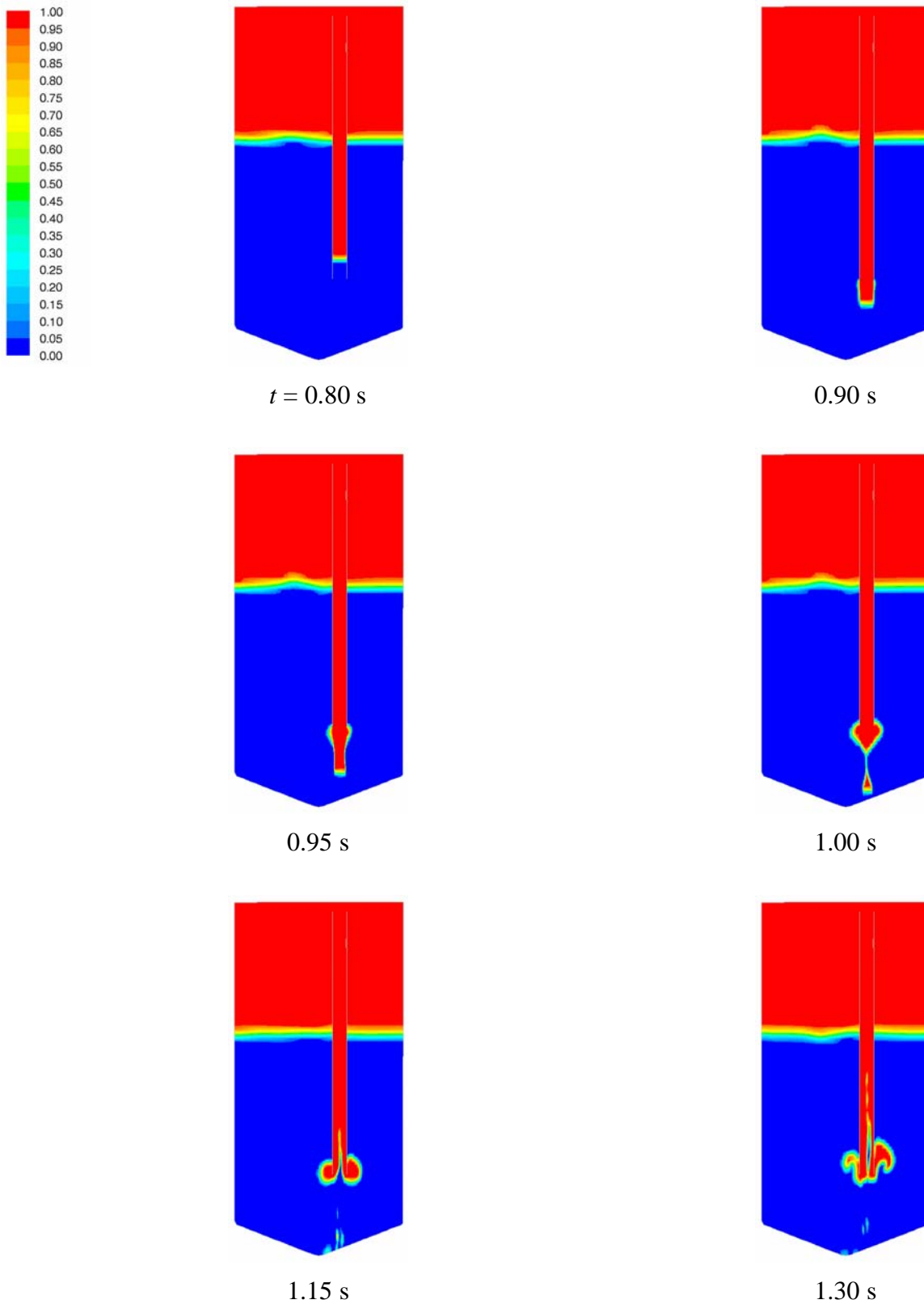


Figure 16. Volume fraction of air in the beginning of the blowdown of air calculated with one-directional fluid-structure coupling. Result obtained with the incompressible VOF model is shown.

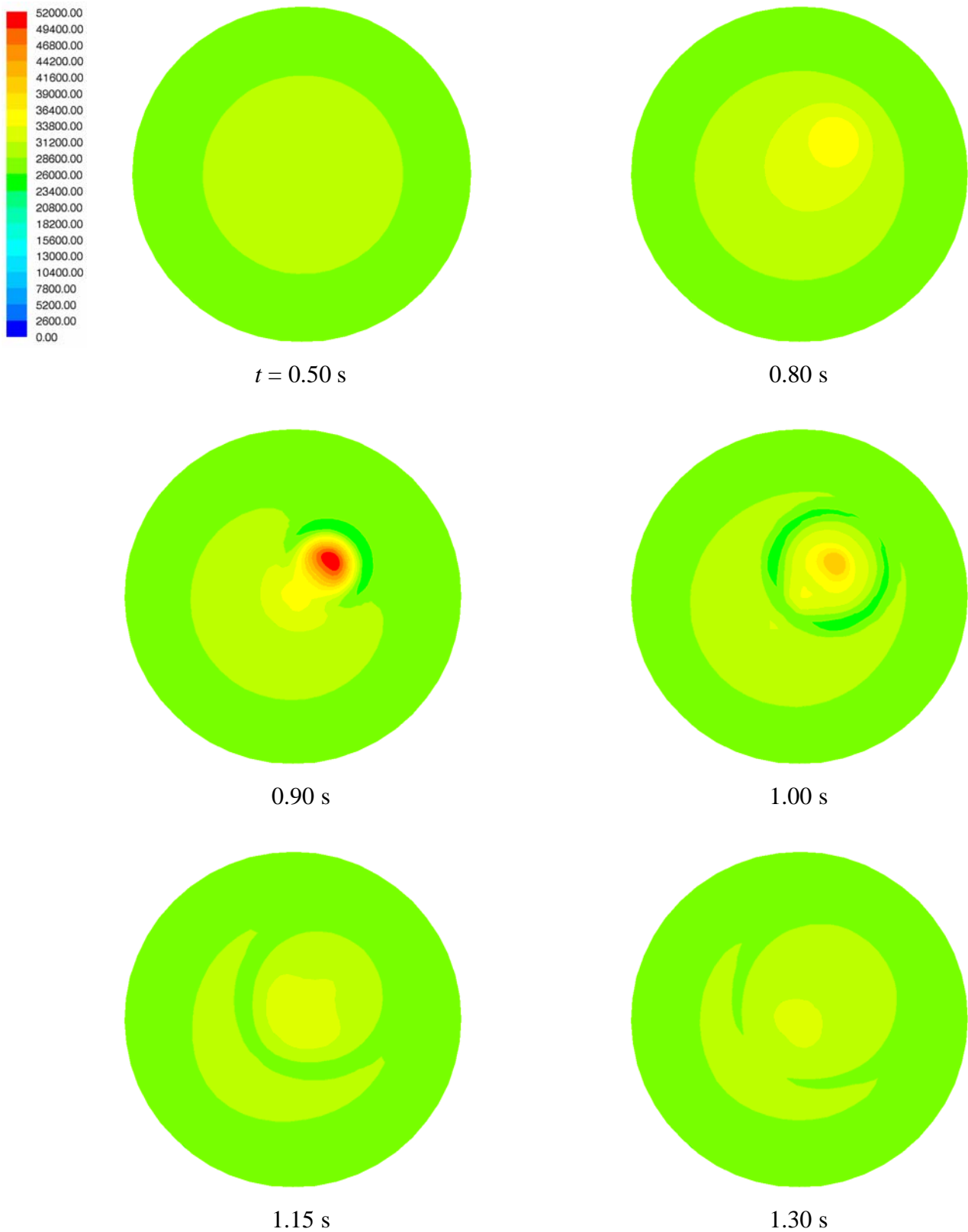


Figure 17. Relative static pressure (Pa) on the pool wall in the beginning of the blowdown of air calculated with one-directional fluid-structure coupling. Result obtained with the incompressible VOF model is shown. Relative static pressure at the top of the pool is zero.

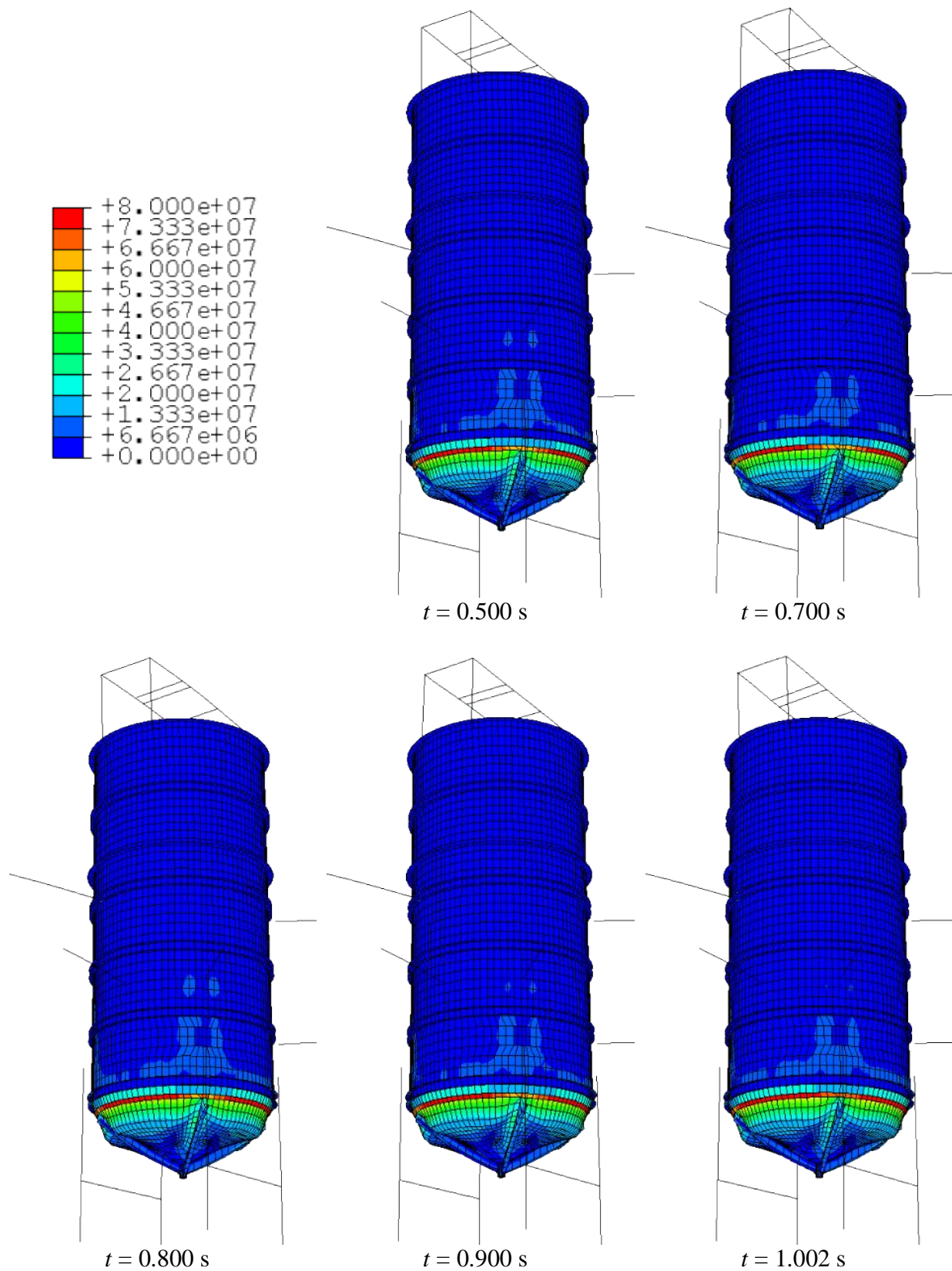


Figure 18. Von Mises stress (Pa) on the inner surface in the beginning of the blowdown of air calculated with one-directional fluid-structure coupling. Result obtained with the incompressible VOF model is shown. The deformation scale factor is 200.

4.1.3.2 Simulation with Compressible VOF Model

In the simulation with the compressible VOF model, air is treated as an ideal gas. When the blowdown begins at $t = 0.50$ s, air in the pipe is compressed and acts like a spring. In Fig. 19, we can see that the water plug is expelled from the pipe at time $t = 0.88$ s. The accelerated water plug hits the pool bottom in the time interval 0.85...0.95 s. The air jet following the water plug reaches the pool bottom at $t = 0.95$ s. The expelled water hits back into the pipe in the time interval 1.0 ... 1.2 s and a jet of water penetrates into the pipe.

In the compressible simulation, the velocity of the water plug leaving the pipe was about 13 m/s. Thus, the velocity of the expelled water is two times the velocity found in the incompressible simulation. The difference is caused by energy stored in compressed air in the early phase of the simulation.

The pressure load on the pool bottom is shown in Fig. 20. In steady state, the maximum hydrostatic pressure in the pool with 3.2 m of water is 37 kPa. When the blowdown starts at $t = 0.50$ s, the pressure rises in the pipe and also in the pool bottom. At time $t = 0.90$ s, the maximum value of the pressure is already about 50 kPa at the pool bottom.

The maximum load on the pool bottom occurs in the time interval 0.90 ... 1.10 s. First, a pressure maximum occurs at $t = 0.90$ s, when the water plug hits the pool bottom. Second, a pressure minimum occurs at $t = 0.95$ s, when the air jet following the water plug reaches the bottom of the pool. Very small values of pressure between 3 and 5 kPa are found at the pool bottom at this time. Third, the pressure rises again very rapidly at time $t = 1.00$ s, when water is flowing back towards the pipe outlet. The maximum value of pressure at this time is 73 kPa. Then pressure continues oscillating with decreasing amplitude.

Von Mises stress on the inner wall of the pool is shown in Fig. 21. In steady state, the maximum value at the rounding of the pool bottom is about 76 MPa. During the oscillating load, in time interval 0.90...1.10 s, the maximum stress value is about 103 MPa.

The pressure loads in the incompressible and compressible simulations are compared in Fig. 22. The pressure load at the pool bottom obtained with the incompressible simulation has the spurious pressure peak at time $t = 0.538$ s. After this the pressure increases steadily and reaches a maximum value of about 48 kPa at time $t = 0.90$ s. The pressure load obtained with the compressible simulation oscillates rapidly and has two maxima with magnitude larger than 70 kPa. A minimum with a pressure of about 10 kPa occurs between the maxima.

The vertical displacement of the pool bottom in the incompressible and compressible simulations is compared in Fig. 23. In both simulations, the initial oscillation due to the application of the pressure load damps in approximately 0.5 s. The reason for the high frequency of the oscillations is the one-directional coupling, i.e., the mass of water does not participate in the oscillation. The spurious pressure peak in the incompressible simulation causes another oscillation $t = 0.538$ s. After $t = 0.90$ s, the actual pressure load can be resolved from the curve. Very little high-frequency oscillations occur in the compressible simulation, since the pressure load with compressible air has no sharp peaks.

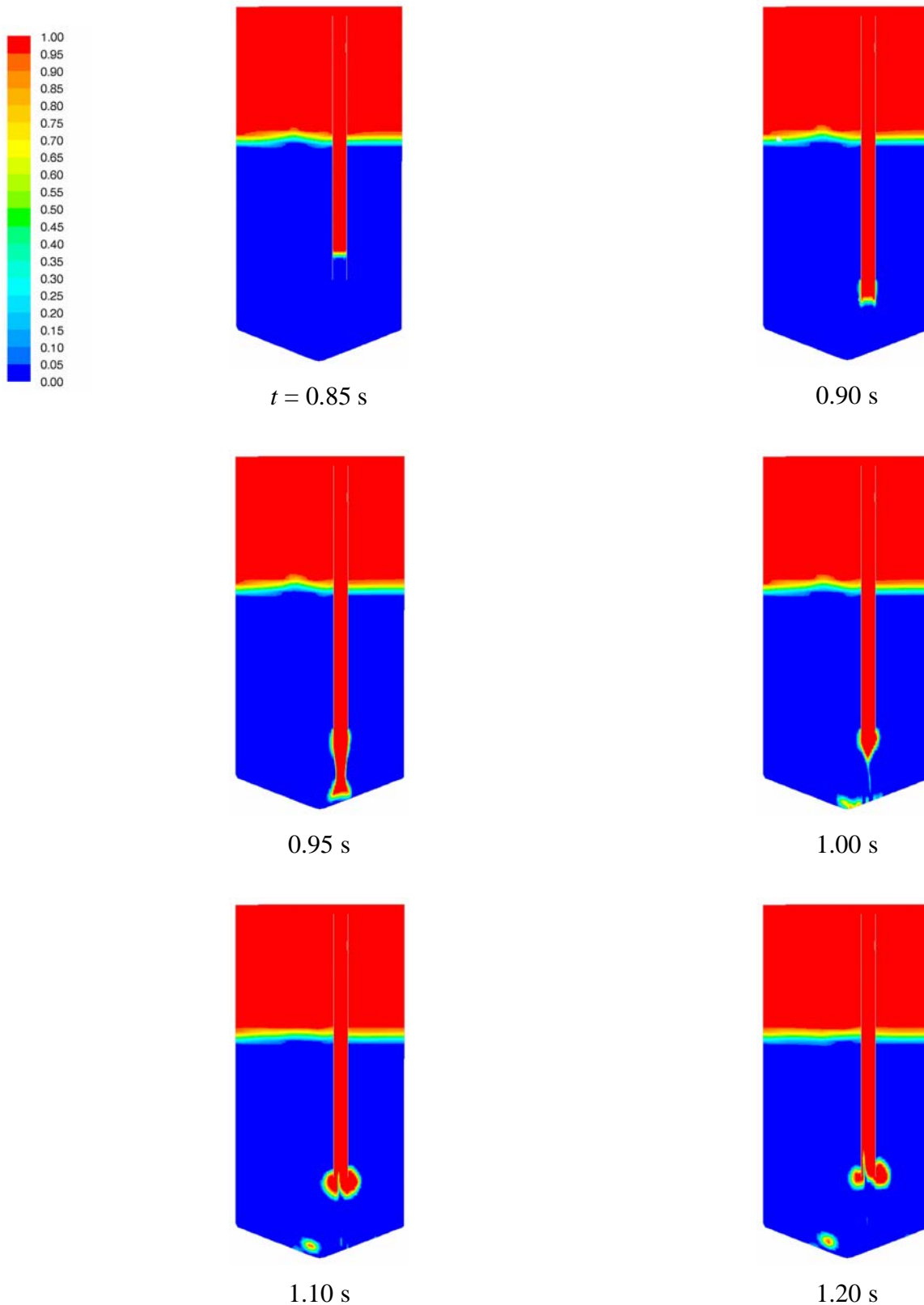


Figure 19. Volume fraction of air in a cross-section of the pool in the beginning of the blowdown of air calculated with one-directional fluid-structure coupling. Result obtained with the compressible VOF model is shown.

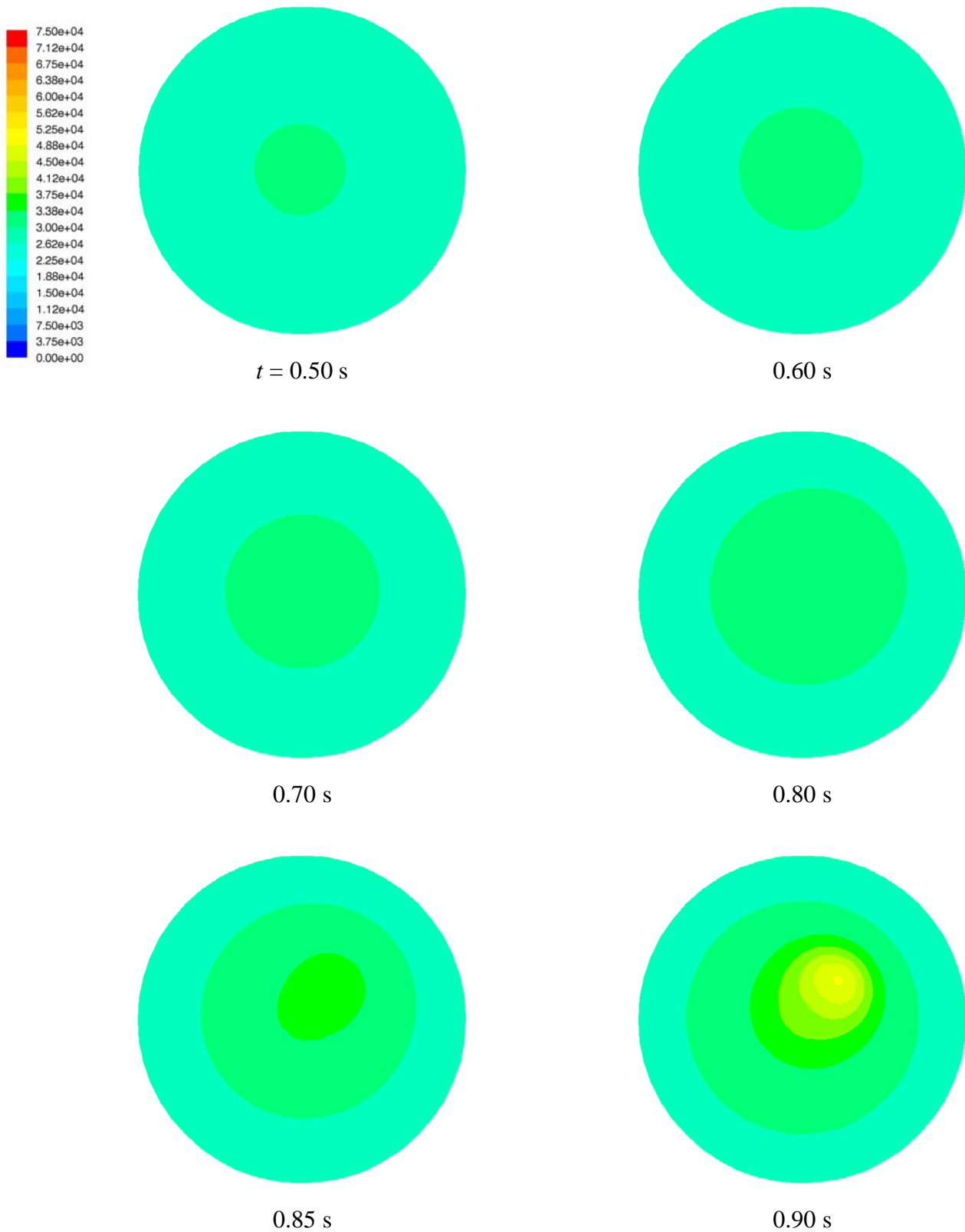


Figure 20. Relative static pressure (Pa) on the pool bottom in the beginning of the blowdown of air calculated with one-directional fluid-structure coupling. Result obtained with the compressible VOF model is show. Relative static pressure at the top of the pool is zero (continues on the following page).

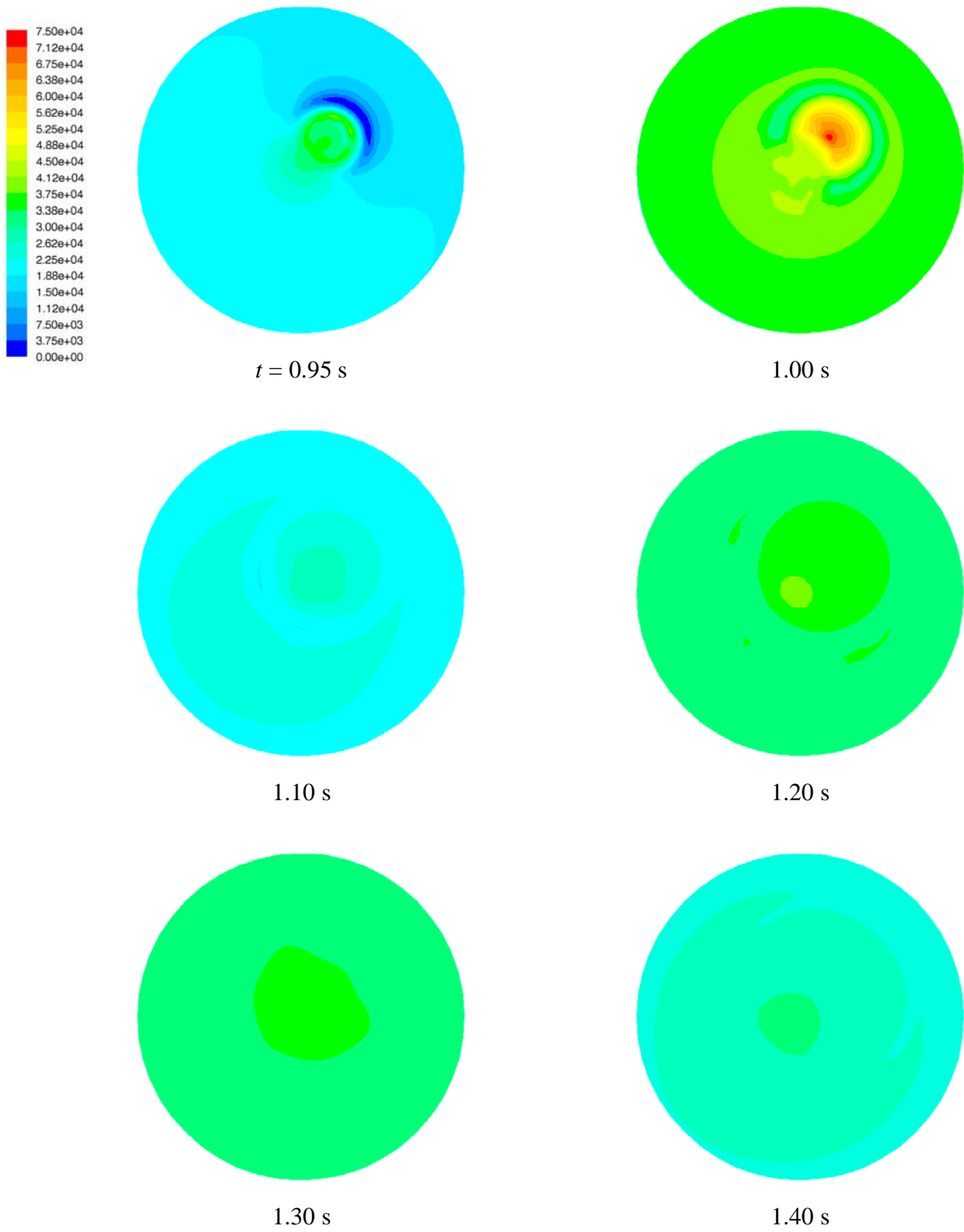


Figure 20. Continues from the previous page.

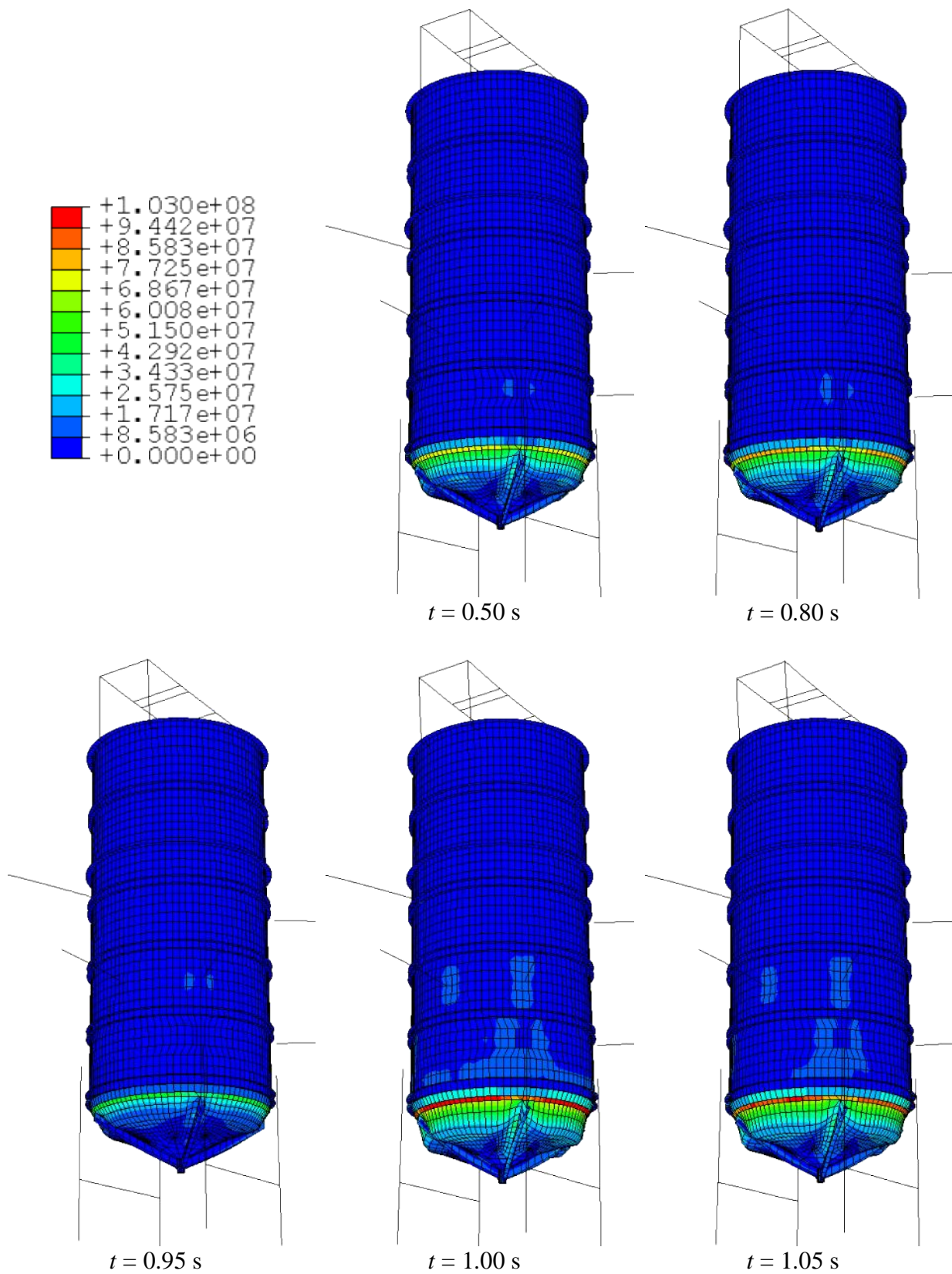


Figure 21. Von Mises stress (Pa) on the inner surface in the beginning of the blowdown of air calculated with one-directional fluid-structure coupling. Result obtained with the compressible VOF model is shown. The deformation scale factor is 200.

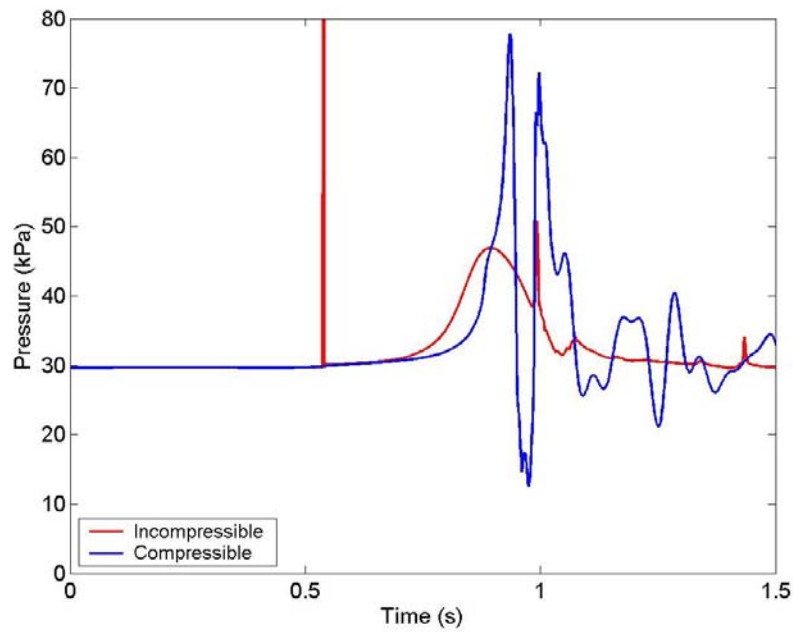


Figure 22. Relative static pressure (kPa) in simulations with incompressible and compressible VOF models. Pressure is plotted at the intersection point of the pipe axis and the pool bottom.

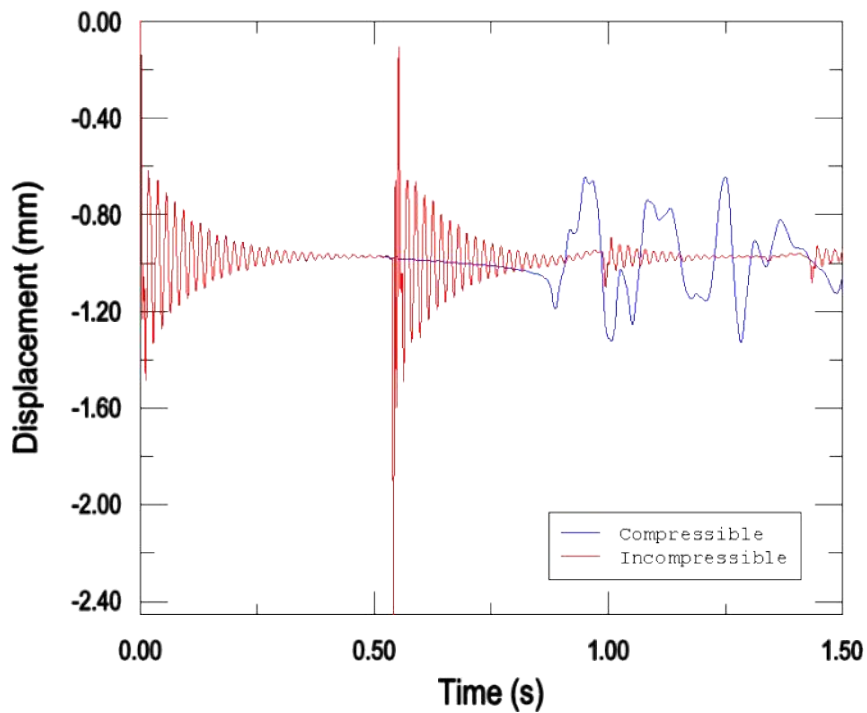


Figure 23. Vertical displacement (mm) of the bottom centre of the pool in simulations with incompressible and compressible VOF models.

4.2 Fluid-structure Calculations with Star-CD and ABAQUS

In this section, the fluid-structure interaction calculations carried out with Star-CD and ABAQUS are described. The internal ES-FSI code of Star-CD was used for coupling the flow and structural analysis.

4.2.1 ES-FSI Code

ES-FSI allows FSI analysis without the need of simultaneous coupling of CFD and FE codes. The reduced structural model matrices are first calculated with the FE code. These matrices are then used by ES-FSI to solve the motion of the structure during the CFD calculation. The CFD mesh is moved according to the displacements of the structure. In the final step, these displacements are used for post-processing the structure.

In the method used by ES-FSI, the behaviour of the structure is assumed to be fully linear. In addition, the memory requirement becomes too large for many practical applications. This is due to the substructure analysis required for the current version of ES-FSI. The ES-FSI code and substructure analysis are presented in more detail by Pättikangas et al. (2005).

4.2.2 CFD and Structural Models

The CFD and structural models presented in Fig. 12 were used for the analysis with ES-FSI. Only the bottom part of the pool was selected as the coupling surface in order to save computational effort. In order to increase the accuracy of the dynamic response of the substructure, nodes also above the coupling surface were retained. The surfaces on which pressures and displacements are coupled are shown in Fig. 24. Fig. 24 also shows the master nodes of the substructure.

In this work, the motion of the internal CFD mesh was handled by using a Pro-Star pre-processor macro. Only the translational DOF of the structure were retained since ES-FSI allows currently only translational DOF. However, the effect of including also the rotational DOF to the substructure of the pool was shown to be negligible by Pättikangas et al. (2005). The motion of the structure was solved once in each CFD time step.

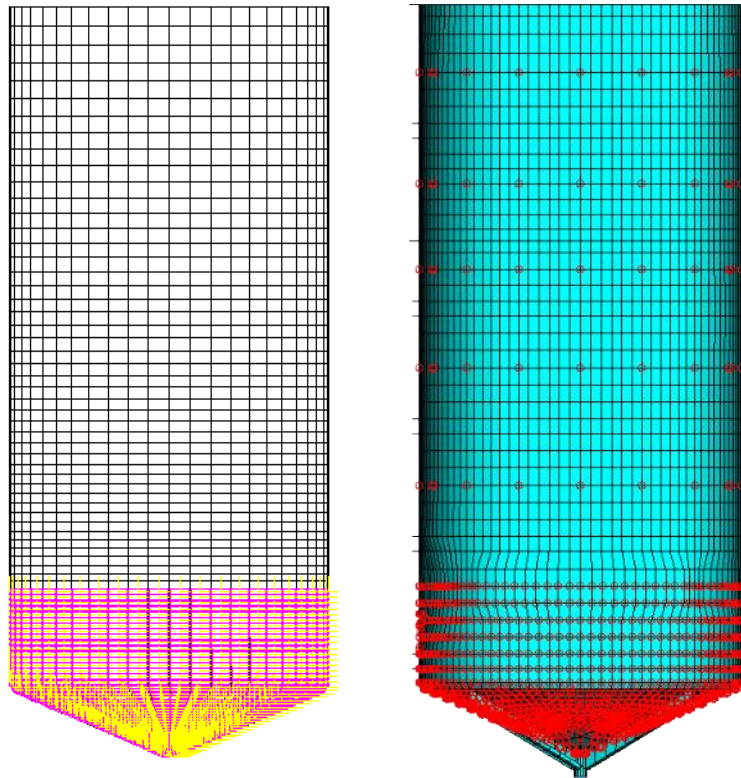


Figure 24. Coupling surfaces on CFD and structural meshes and master nodes used in analysis with ES-FSI.

4.2.3 Simulation of the POOLEX Experiment

The experiment chosen for the calculation with ES-FSI was STB-17-6 (see Laine and Puustinen, 2005). In the experiment series STB-17, largest steam generator pressures were used and also largest strains were measured from the pool wall. The largest strains were due to the water plug hit on the pool bottom in the beginning of the blowdown. The condensation of steam starts rapidly after the initiation of the blowdown and can not be presently correctly modelled. Therefore, the aim of the present analysis was to calculate only the early phase of the experiment where the water plug is expelled from the pipe. It should be noted that in the experiment STB-17-6, the blowdown pipe was initially filled with steam (Puustinen, 2005a), which means that significant condensation may occur already inside the pipe.

The Volume Of Fluid (VOF) model of Star-CD version 3.15 was used in the calculation. Therefore, both steam and water were assumed as incompressible. A pressure boundary condition was applied at the pipe inlet, where measured pressure was used. The pressure used in the inlet is shown as a function of time in Fig. 25. As can be seen from Fig. 25, the blowdown pressure is quite high and therefore the approximation of incompressible gas might not be a very good one. The standard large Reynolds number $k-\varepsilon$ model was used for modelling the turbulence.

The calculation with ES-FSI was first attempted by using two-directional coupling. In this case, however, the calculation became unstable already at an early stage. With two-directional coupling, amplitude of a small oscillation of the pool started to grow rapidly leading to termination of the analysis. With single-phase flow and compressible water, the calculation remained stable for much longer but became eventually unstable as well. Due to the instabilities, the calculation was carried out by using one-directional coupling, i.e., only the

pressures were transferred to the structure and the boundaries of the CFD mesh were non-deforming.

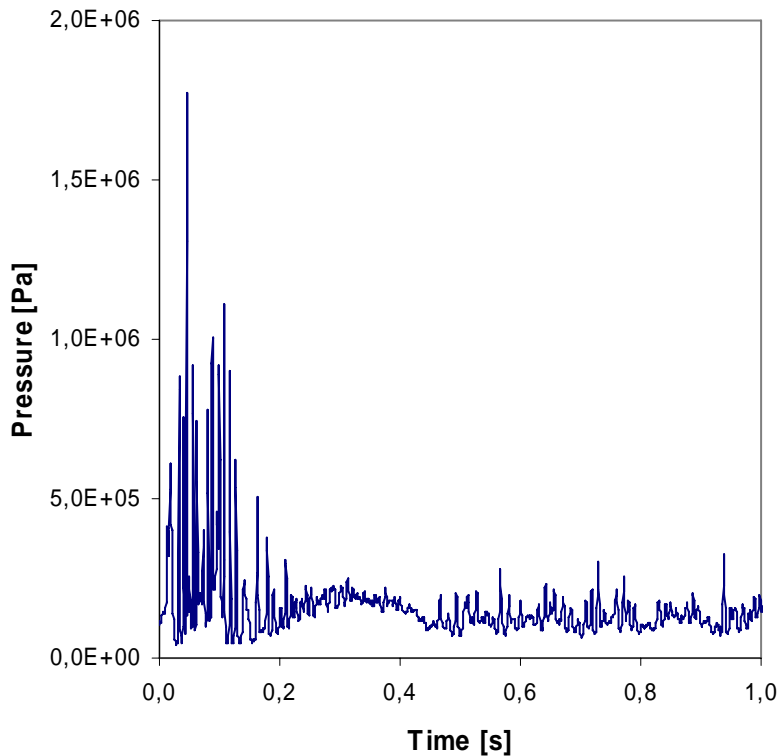


Figure 25. Measured pressure inside the blowdown pipe as a function of time for the POOLEX experiment STB-17-6. The pressure is measured at the location of the initial water level (pressure transducer P3 in Laine and Puustinen, 2005). The blowdown was initiated at $t = 0$.

4.2.4 Results for One-directional FSI Simulation

Volume fraction of water in the pool at selected instants of time is presented in Fig. 26 for the one-directional simulation. At $t = 0$, steam starts to push the water column in the pipe downwards. It can be seen that water is completely expelled from the pipe at approximately $t = 0.22$ s. After this, a large bubble is formed at the pipe outlet due to the high blowdown pressure and absence of condensation.

The location of the steam-water interface for the experiment at selected instants of time is shown in Fig. 27. It can be seen from Fig. 27 that the interface reaches the pipe outlet at about $t = 0.36$ s, whereas the corresponding instant of time in the simulation is about $t = 0.22$ s. The fact that no large bubble is formed in the experiment, contrary to the simulation, indicates that the condensation of steam is very rapid already in the beginning of the blowdown. In the experiment, the steam-water interface starts to move back towards the pipe outlet at about $t = 0.44$ s. The lag of the steam-water interface in the experiment compared to the simulation might be due to condensation of steam already inside the pipe. In addition, the assumption of incompressible gas may in part cause the above mentioned differences between the experiment and simulation.

Fig. 28 presents the inner surface von Mises stress distribution and the deformed shape of the pool at selected instants of time. The maximum value at the rounding of the pool bottom due

to hydrostatic load is about 75 MPa. The maximum von Mises stress during the simulation is approximately 400 MPa. The maximum stress occurs at about $t = 0.3$ s at the rounding of the pool bottom.

Pressure on the bottom of the pool for the experiment and for the CFD calculation is plotted in Fig. 29. The more rapid pressure rise in the simulation compared to the experiment might be due to the used assumption of incompressible and non-condensable gas. The pressure peak caused by the water plug hit on the pool bottom is at least of right order in the simulation.

Stress near the bottom rounding of the pool for the experiment and for the simulation is shown in Fig. 30. The high-frequency oscillation in the simulation is due to the used one-directional coupling, i.e. the pool oscillates as if it were in vacuum. Again in this case, the peak stress due to the water plug hit on the pool bottom is of right order in the simulation. It is interesting to note, however, that the first large stress peak in the experiment has an opposite sign compared to the simulation.

Note that there is not much use comparing the pressure and stress curves in Figs. 29 and 30 after the water plug has been expelled from the pipe. This is due to the large differences between the experiment and simulation in the late phase of the blowdown (see Figs. 26 and 27).

The velocity of the steam-water interface as it exits the pipe, estimated from the frame captures shown in Fig. 27, is approximately 15 m/s. Although not shown, the corresponding value for the CFD calculation is about 14 m/s, which is quite close to the experiment.

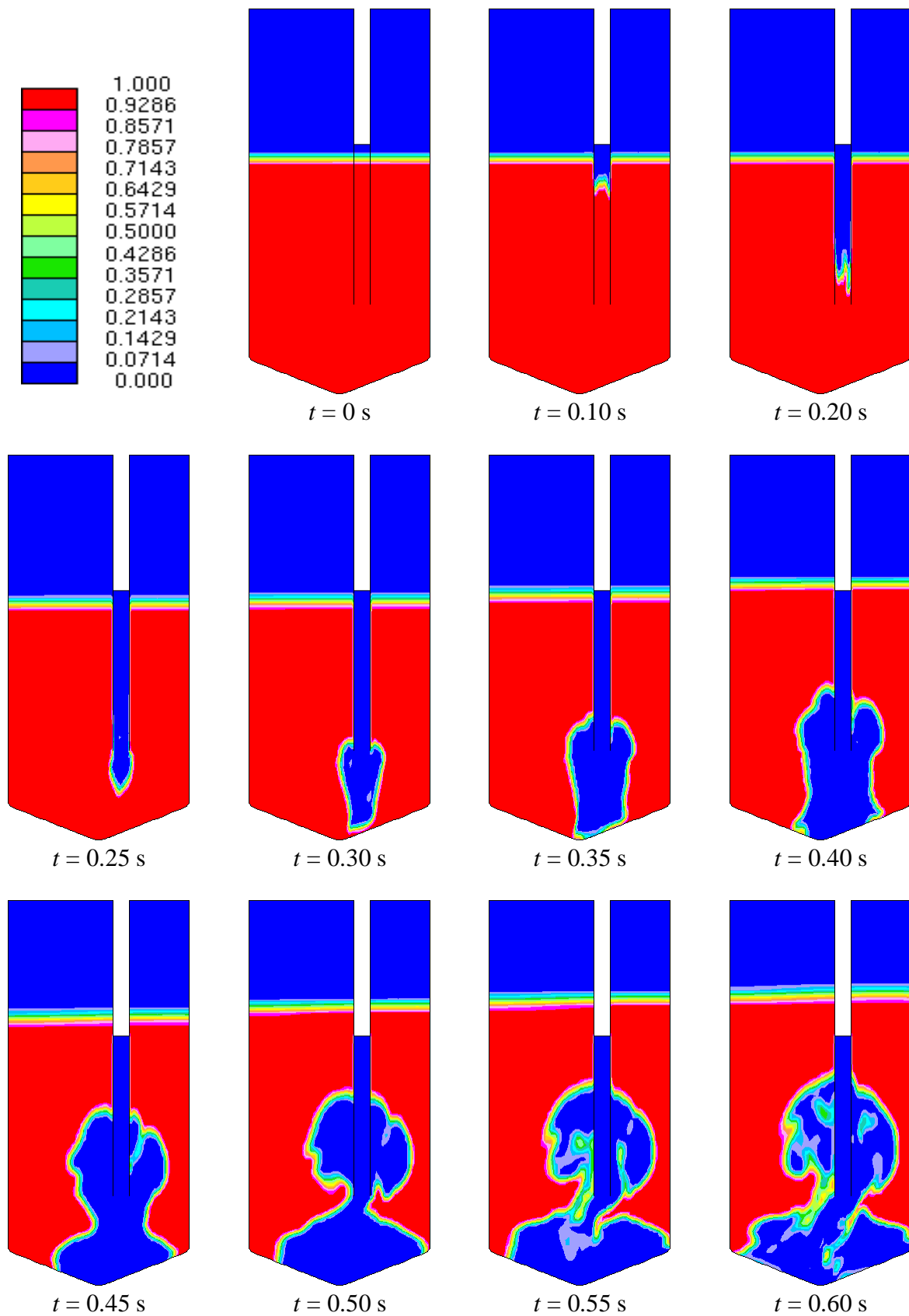


Figure 26. Volume fraction of water in a vertical cross-section of the pool at different instants of time for the one-directional calculation with ES-FSI.

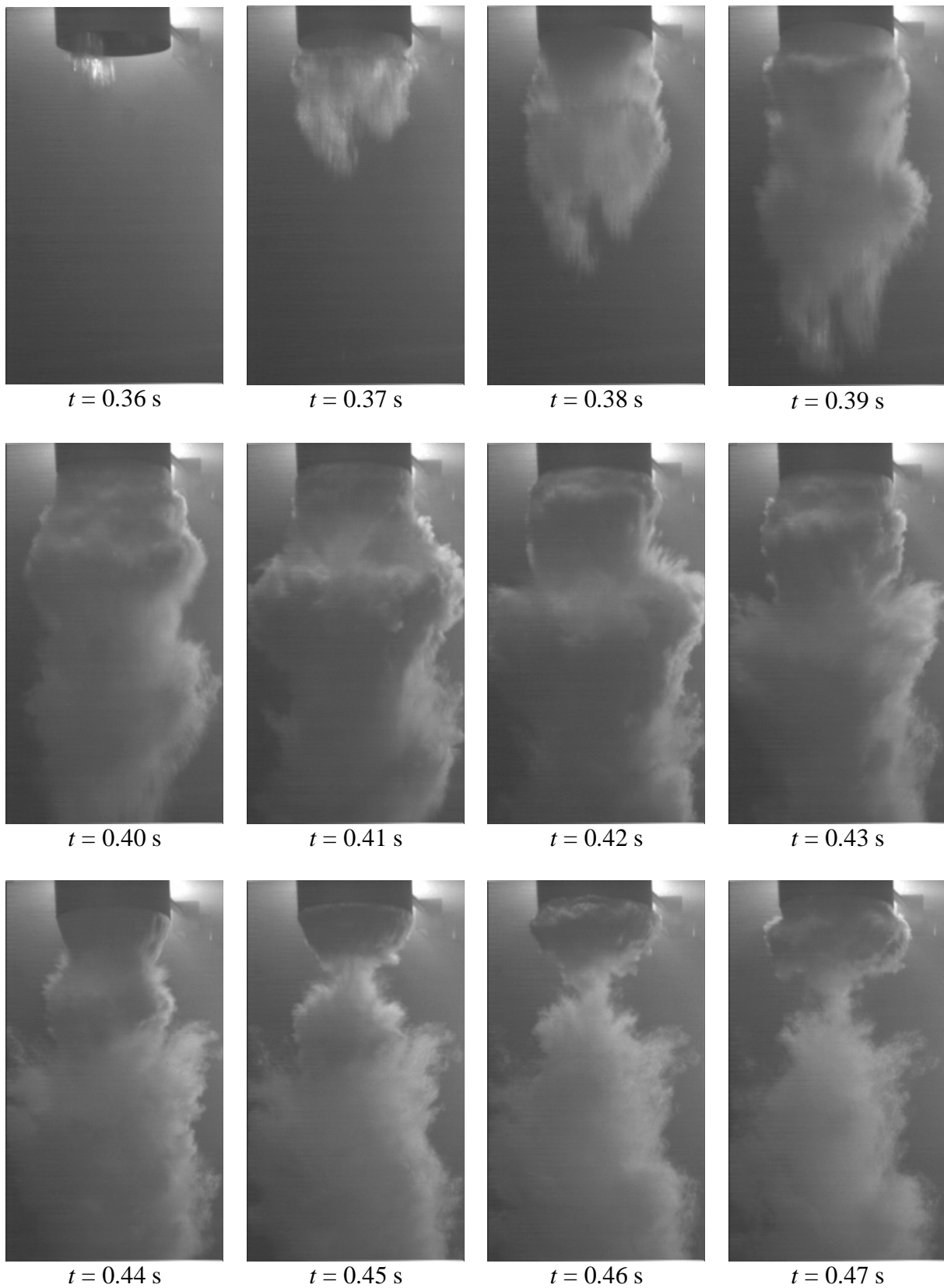


Figure 27. Frame captures from the POOLEX experiment STB-17-6 at different instants of time.

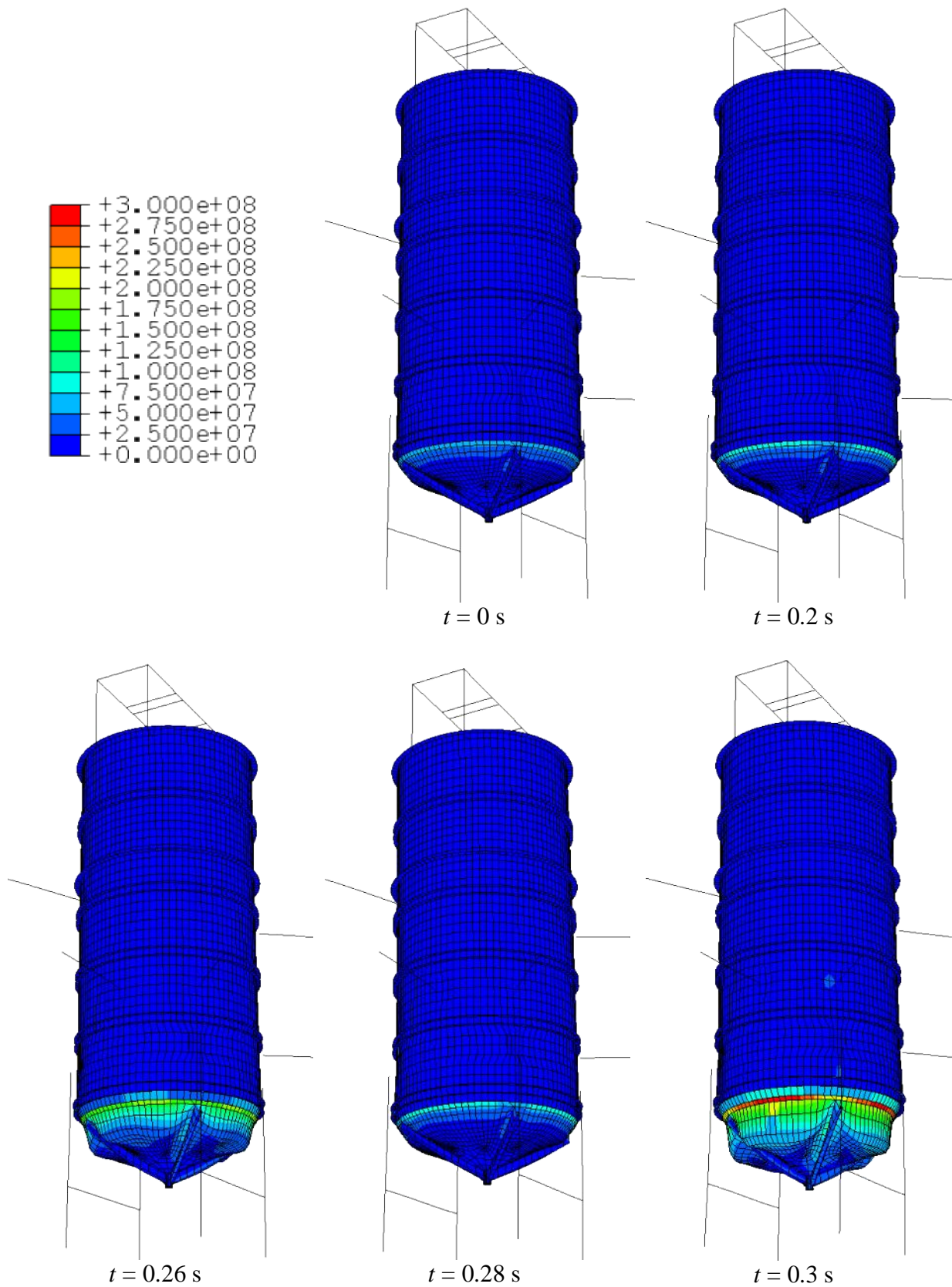


Figure 28. Von Mises stress (Pa) on the inner surface at different instants of time for the one-directional calculation with ES-FSI. The deformation scale factor is 100.

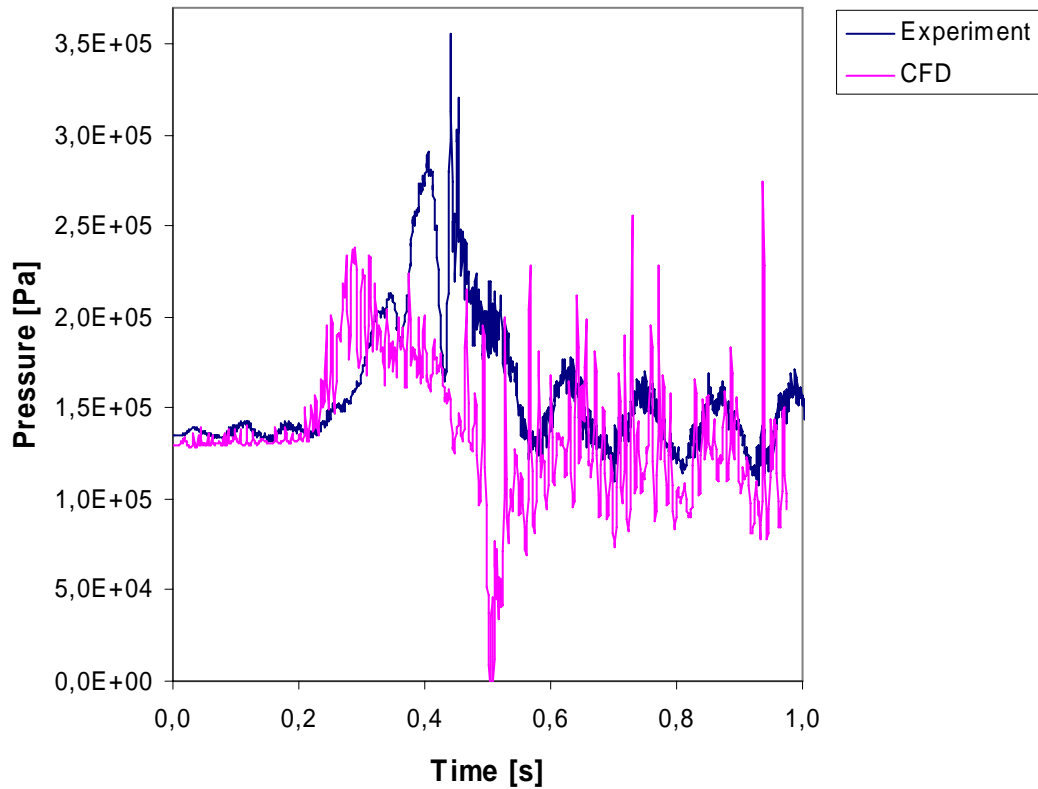


Figure 29. Pressure on the bottom of the pool as a function of time for the POOLEX experiment STB-17-6 and for the one-directional calculation with ES-FSI.

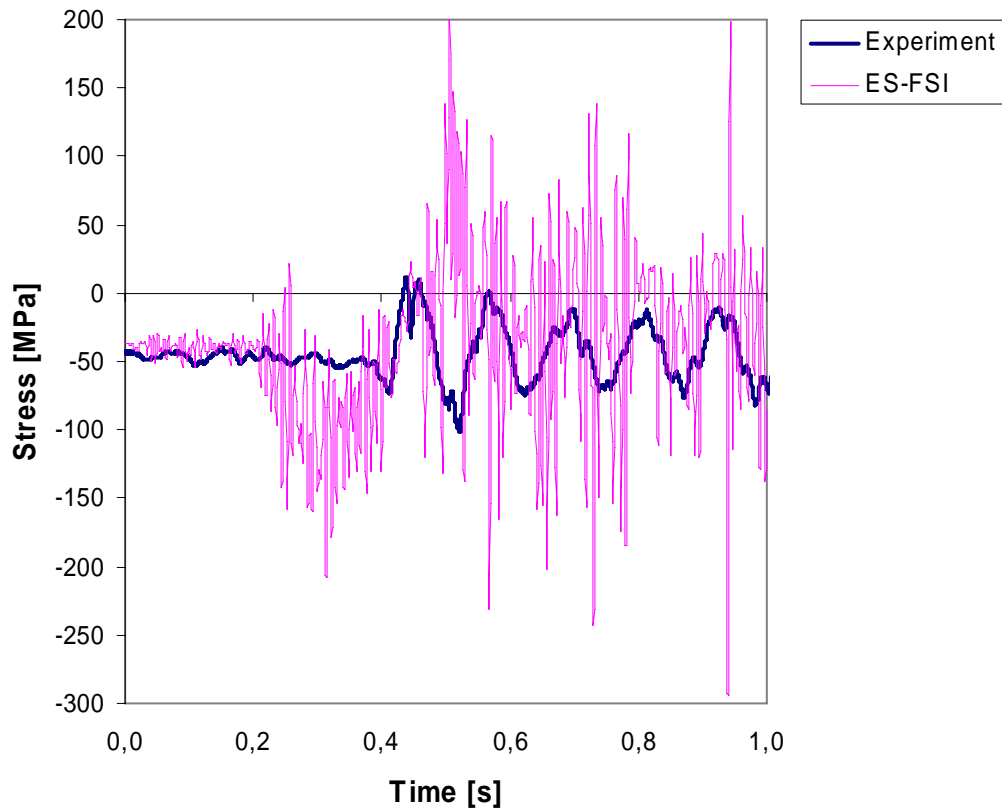


Figure 30. Hoop stress near the bottom rounding of the pool as a function of time for the POOLEX experiment STB-17-6 and for the one-directional calculation with ES-FSI.

5 Coupled Acoustic-structural Analyses with ABAQUS

The coupled fluid-structure calculations performed with ABAQUS are described in the following. The equations governing an acoustic problem with a moving boundary are first presented in Sec. 5.1. After this, the effect of compressibility of the fluid is discussed in Sec. 5.2. Calculations for a two-dimensional test case are presented in Sec. 5.3. The results obtained with ABAQUS are compared to analytical results and to results obtained with another FE code. Both compressible and incompressible fluid is considered in the reference solutions. In Sec. 5.4, calculations with ABAQUS are compared to experimental results in another test case. Another FE solution, in which the assumption of incompressible fluid is used, is included for comparison. Calculations for the pool and a brief comparison with the POOLEX experiments are presented in Sec. 5.5. The calculations presented in this section consist of eigenvalue extractions for the coupled systems.

5.1 Governing Equations

The equations governing a coupled acoustic-structural problem are presented in ABAQUS (2004). The equilibrium equation for the fluid is

$$\nabla p + \rho \mathbf{u} = 0, \quad (14)$$

where p is the pressure in the fluid in excess of any static pressure, ρ is the density of the fluid and \mathbf{u} is the acceleration of the fluid particle. A linear inviscid constitutive behaviour is assumed for the fluid:

$$p = -K \nabla \cdot \mathbf{u}, \quad (15)$$

where K is the bulk modulus of the fluid and \mathbf{u} is the displacement of the fluid particle.

On the fluid-structure interface, pressures and displacements normal to the interface are coupled. The acceleration of the interface affects the boundary condition of the acoustic domain by equation

$$\rho \mathbf{n} \cdot \mathbf{u} = -\mathbf{n} \cdot \nabla p, \quad (16)$$

where \mathbf{n} is the normal vector of the interface. On a rigid boundary, we have $\mathbf{u} = 0$ and

$$\mathbf{n} \cdot \nabla p = 0. \quad (17)$$

5.2 Effect of Compressibility of the Fluid

When calculating coupled eigenmodes of a fluid-structure system, practically identical results are obtained in certain cases with acoustic and incompressible flow calculations (Junger and Feit, 1986; Yu, 1987). In the acoustic approach, the fluid is represented as stagnant but compressible. In the other case, a flowing but incompressible fluid is used.

For a two-dimensional cylinder filled with fluid, described in the following section, the condition for which either the acoustic or incompressible flow approach may be used is (Yu, 1987)

$$\frac{\omega a}{c} \ll 1, \quad (18)$$

where ω is the eigenfrequency of the coupled system, a is the radius of the cylinder and c is the speed of sound in the fluid. Condition (18) states that compressibility may be ignored if the wave length is large compared to the radius of the cylinder.

The theory of coupled acoustic-structural systems is presented thoroughly by Junger and Feit (1986). Their work indicates that the condition (18) is more general, but this kind of general condition is not clearly presented by Junger and Feit (1986). The general condition would mean that for a fluid surrounded by a flexible structure, the radius a in (18) could be replaced with l , the characteristic length of the structure. Therefore, the theory presented by Junger and Feit (1986) is worth studying in future work. The general condition would be useful also outside the scope of this work. For example, in analysing transverse vibrations of fluid filled pipes, the condition could be used for examining whether the simple added mass (incompressible) approximation can be used.

5.3 Calculations for a Two-dimensional Test Case

In this section, a test case presented in Yu (1987) is considered. Eigenmodes obtained with ABAQUS are compared to analytical results and to results obtained with the WECAN FE code (Yu, 1987).

5.3.1 Problem Description

The problem consists of a fluid filled cylinder. A two-dimensional case is assumed, i.e. the axial displacement is zero and the radial and circumferential displacements are independent of the axial coordinate. The parameters of the problem are listed in Table 1.

Table 1. Dimensions and material properties for the two-dimensional fluid filled cylinder (Yu, 1987).

Cylinder	Mean Radius a [m]	1.575
	Wall Thickness t [m]	0.102
	Young's Modulus E [GPa]	206.8
	Poisson's ratio	0
	Density ρ_s [kg/m³]	2403
Fluid	Bulk Modulus K [GPa]	2.25
	Density ρ_f [kg/m³]	1000

5.3.2 FE Model for ABAQUS Calculations

The wall of the cylinder was modelled with 8-node quadrilateral shell elements with a side length of approximately 200 mm. Hexahedral 20-node acoustic elements were used for the fluid. The type and number of elements used in the model are listed in Table 2. The mesh of the model is shown in Fig. 31.

Table 2. Type and number of elements used in the FE model of the two-dimensional cylinder.

Region	Element type	Description	No. of elements
Cylinder	S8R	8-node doubly curved thick shell, reduced integration	49
Fluid	AC3D20	20-node quadratic brick	414

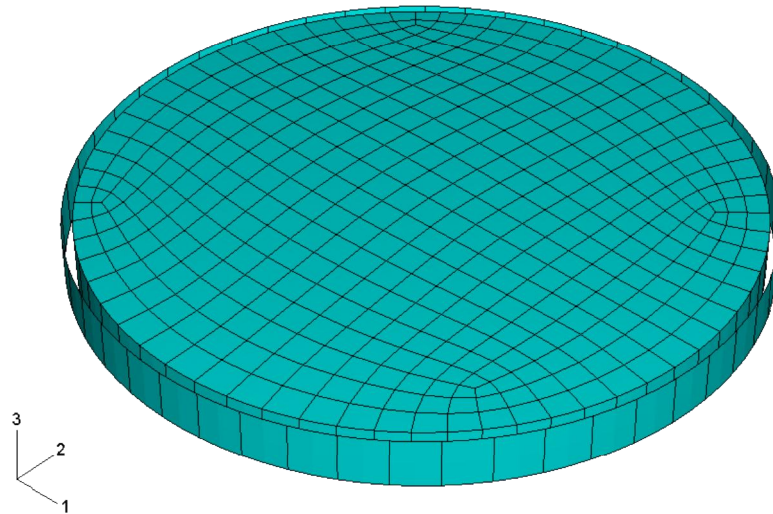


Figure 31. Mesh of the FE model of the two-dimensional cylinder filled with fluid.

5.3.3 Results of Eigenvalue Extraction

Frequencies of the first 10 eigenmodes of the cylinder are listed in Table 3 for the different calculations. Mode shapes of the eigenmodes are presented in Fig. 32. Due to symmetry, eigenmodes with the same number of waves n around the circumference are in pairs having same frequency but different orientation. It may be concluded that the agreement between the results of the three different calculations is good for the case in which the cylinder is in vacuum and for the case in which the cylinder is filled with compressible fluid. The frequencies with the assumption of incompressible fluid are higher than those obtained by using compressible fluid. At lower frequencies, however, the results with compressible and incompressible fluid are very close to one another. It can be seen that the effect of compressibility increases with increasing frequency as indicated by the condition (18) in Sec. 5.2. For this case, the dimensionless parameter in the condition equals approximately 0.17 for the lowest mode.

Table 3. Frequencies (Hz) of the first 10 eigenmodes of the two-dimensional cylinder for different calculations (see also Fig. 32). The analytical results and the results obtained with the WECAN FE code are from Yu, (1987).

n	Cylinder in Vacuum			Compressible Fluid			Incompressible Fluid	
	Analytical	ABAQUS	WECAN	Analytical	ABAQUS	WECAN	Analytical	WECAN
2	46.843	46.912	46.808	25.038	25.408	25.308	25.057	25.327
3	132.48	132.30	132.11	77.924	78.799	78.554	78.189	78.822
4	254.00	252.65	252.54	160.42	161.52	161.20	161.71	162.49
5	410.75	406.55	406.93	272.99	273.45	273.34	277.00	277.31
6	602.56	592.91	594.49	415.17	413.64	414.24	424.92	423.75

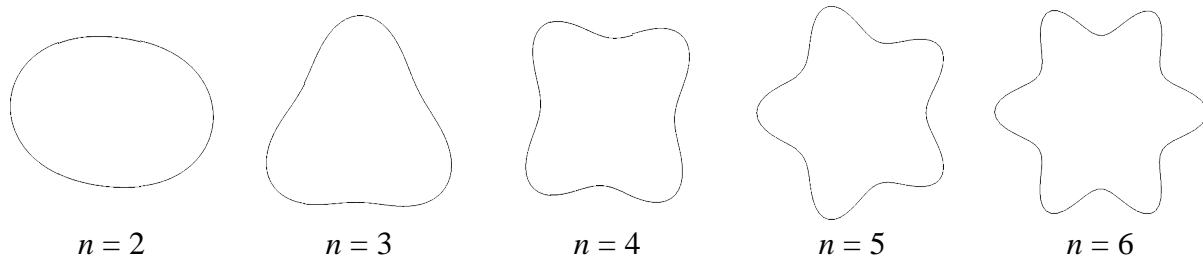


Figure 32. Mode shapes of the first 10 eigenmodes for the two-dimensional fluid filled cylinder. Note that eigenmodes with the same number of waves n around the circumference are in pairs due to symmetry.

5.4 Calculations for a Three-dimensional Test Case

The experimental and numerical study of a steel cylinder filled with water, presented in Mazúch et al. (1996), is considered in this section. In the FE analysis of the cylinder carried out by Mazúch et al. (1996), water was modelled by using the potential flow theory (see Sec. 2.3). In other words, water was assumed as incompressible and inviscid in the reference calculation.

5.4.1 Problem Description

The problem consists of a vertical cylinder filled with water. The top of the cylinder is open and the bottom is assumed to be fully rigid. In this work, only the case where the cylinder is completely filled is studied although Mazúch et al. (1996) examined cases with varying water level. In addition, eigenmodes of the empty cylinder are calculated and compared to the reference results in order to validate the structural model. The dimensions and material properties for the cylinder are listed in Table 4. The material properties for water were not available in the reference and for this work values $K = 2.165$ GPa and $\rho = 1000$ kg/m³ were assumed for bulk modulus and density, respectively.

Table 4. Dimensions and material properties of the cylinder examined by Mazúch et al. (1996).

Mean Radius a [mm]	77.25
Wall Thickness t [mm]	1.5
Height h [mm]	231
Young's Modulus E [GPa]	205
Poisson's ratio	0.3
Density ρ [kg/m ³]	7800

5.4.2 FE Model for ABAQUS Calculations

The wall of the cylinder was modelled by using 8-node quadrilateral shell elements with a side length of approximately 14 mm. Hexahedral 20-node acoustic elements were used for water. The side length of the acoustic elements was on the average approximately 10 mm. Symmetry was used and therefore only a half of the cylinder was modelled. The type and number of elements used in the model are listed in Table 5. The mesh of the model is shown in Fig. 33.

Table 5. Type and number of elements used in the FE model of the three-dimensional cylinder.

Region	Element type	Description	No. of elements
Cylinder	S8R	8-node doubly curved thick shell, reduced integration	306
Fluid	AC3D20	20-node quadratic brick	2760

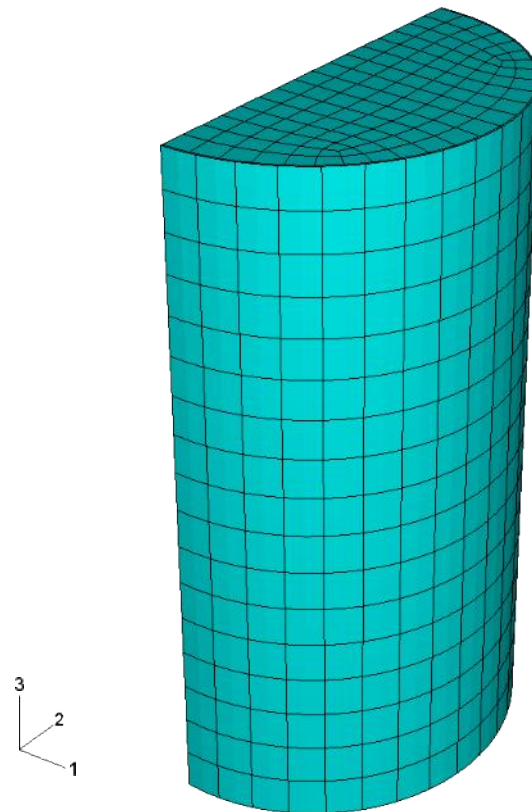


Figure 33. Mesh of the FE model of the three-dimensional cylinder filled with water.

5.4.3 Results of Eigenvalue Extraction

Frequencies of selected eigenmodes of the cylinder for the different calculations and for the experiments are listed in Table 6. Mode shapes of the eigenmodes are shown in Fig. 34. Note that in Table 6 and Fig. 34, the eigenmodes are identified by the axial and circumferential mode shapes m and n , respectively. It can be seen that the agreement between the different calculations is good for the empty cylinder. In the case where water is included, the frequencies of the ABAQUS calculation are expectedly lower compared to the reference FE solution due to the effect of compressibility. In addition, the effect of compressibility increases with increasing frequency which is in accordance with the discussion in Sec. 5.2 and the results in Sec. 5.3. For this problem, the dimensionless parameter in the condition (18) in Sec. 5.2 equals approximately 0.13 for the lowest mode.

The results of the calculations and experiments are close to one another for certain eigenmodes in the case of the empty cylinder. For the same eigenmodes, the agreement between the calculations and experiments with the filled cylinder is relatively good. According to the results, the same sources of error seem to affect the both cases, i.e. the empty and filled cylinder (see for example Mode $m = 1, n = 2$ in Table 6). Mazúch et al. (1996) state that the large differences for Mode $m = 1, n = 2$ may be due to difference in the boundary condition at the bottom edge of the cylinder since this mode is particularly sensitive to the boundary condition.

Table 6. Frequencies (Hz) of selected eigenmodes of the three-dimensional cylinder in the different cases (see also Fig. 34). The experimental and analytical results and the reference FE solution are from Mazúch et al. (1996).

m	n	Cylinder in Vacuum				Cylinder Filled with Water		
		Experiment	Analytical	ABAQUS	Ref. FE Model	Experiment	ABAQUS	Ref. FE Model
1	3	616	633	633.5	633.6	388	397.8	400.6
1	2	708	814	815.0	814.6	421	479.9	482.1
1	4	945	947	947.0	947.6	628	627.4	633.2
1	5	1479	1480	1479.1	1481.1	1027	1021.0	1033.0
2	4	1628	1648	1649.1	1650.3	1094	1098.1	1110.6
1	1	-	1827	1830.1	1826.6	-	1031.0	1038.6
2	5	1851	1839	1837.6	1842.1	1299	1281.6	1304.2
2	3	1969	2029	2032.9	2029.6	1245	1278.1	1286.9
1	6	2151	2154	2153.0	2158.0	1546	1538.0	1561.3
2	6	-	-	2382.8	-	1748	1722.2	1762.6

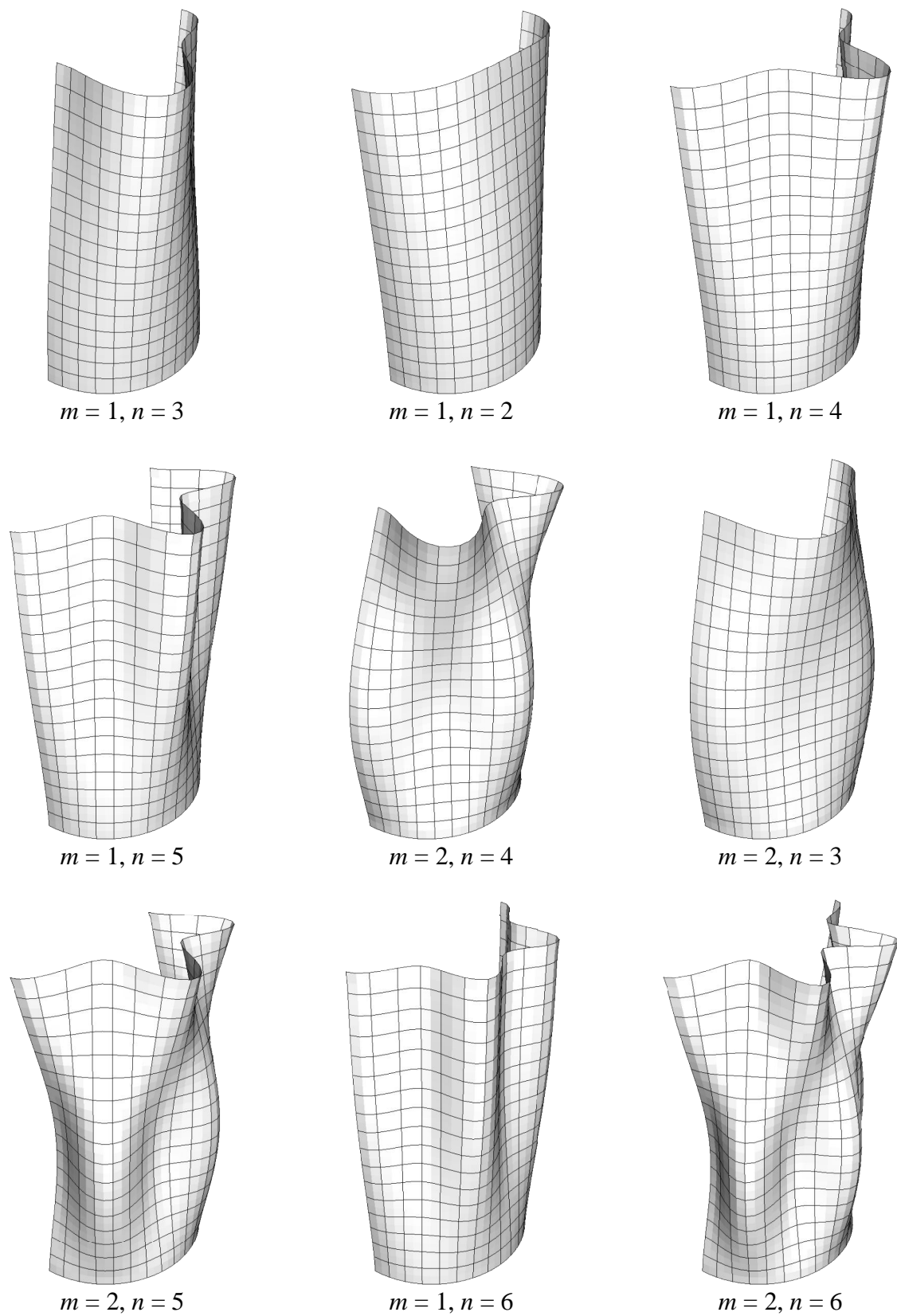


Figure 34. Selected eigenmodes of the three-dimensional cylinder filled with water. Note that the eigenmodes are identified by the axial and circumferential mode shapes m and n , respectively.

5.5 Calculations for the Pool

Eigenvalue extraction was carried out for the pool with the water level of 3.2 m. FE analyses of the pool performed in this work and in the earlier work indicate that the most important mode of oscillation is the vertical motion of the whole bottom of the pool. This motion is due to the flexibility of the wall and disc springs under the supports. This mode seems to be evident also according to the measured strains of the bottom due to the hydrostatic load and during the different experiments (see Laine and Puustinen, 2005). According to the measured strains, the frequency of the oscillation is approximately 10 Hz, which is compared to the coupled FE calculation.

5.5.1 FE Model

The structural model presented in Sec. 4 was used for the pool. For water, the mesh created for the CFD analyses (see Sec. 4) was used. Hexahedral 8-node acoustic elements were applied for the acoustic domain. The type and number of the acoustic elements are presented in Table 7. The material properties used for water are presented in Table 8.

Table 7. Type and number of elements used for water in the coupled acoustic-structural analysis of the pool.

Element type	Description	No. of elements
AC3D8	8-node linear brick	56400

Table 8. Bulk modulus and density used for water in the coupled acoustic-structural analysis of the pool.

Bulk modulus K [GPa]	Density [kg/m ³]
2.165	1000

5.5.2 Results of Eigenvalue Extraction

Frequencies of the first 20 eigenmodes of the pool are listed in Table 9. Selected eigenmodes are shown in Fig. 35. The frequencies of the modes are expectedly clearly lower than the ones calculated for the empty pool in Timperi et al. (2004). In addition, it can be seen that Mode 4 is the oscillation of the pool bottom as discussed above. Note that the shape of the pool bottom in Mode 4 is very similar to the shapes calculated in the dynamic analyses in cases where the pool bottom is pushed downwards by water (see for example Fig. 28). This is expected since Mode 4 takes into account the vertical motion of water. The effective acoustic mass for the eigenmodes is plotted in Fig. 36. It can be seen that the effective acoustic mass for Mode 4 is large compared to the other modes.

The frequency of Mode 4 is approximately 15.7 Hz, which is higher than the measured frequency of 10 Hz. However, the measured displacement of the pool bottom centre in relation to the support beams due to the hydrostatic load was approximately 1.25 mm (Puustinen, 2005b) whereas the corresponding value for the FE model is approximately 0.68 mm. This indicates that the error in the frequency might be mainly due to the too stiff pool bottom in the FE model. The mesh of the FE model is quite coarse at the pool bottom, which is one cause for the too stiff response (Timperi et al., 2004).

Table 9. Frequencies of the first 20 eigenmodes of the pool in the coupled acoustic-structural analysis (see also Fig. 35).

Mode Number	Frequency [Hz]
1	7.765
2	10.99
3	14.10
4	15.70
5	16.14
6	17.41
7	20.39
8	22.93
9	25.81
10	30.04
11	32.32
12	32.48
13	33.66
14	35.55
15	36.10
16	38.51
17	40.33
18	44.14
19	45.04
20	46.69

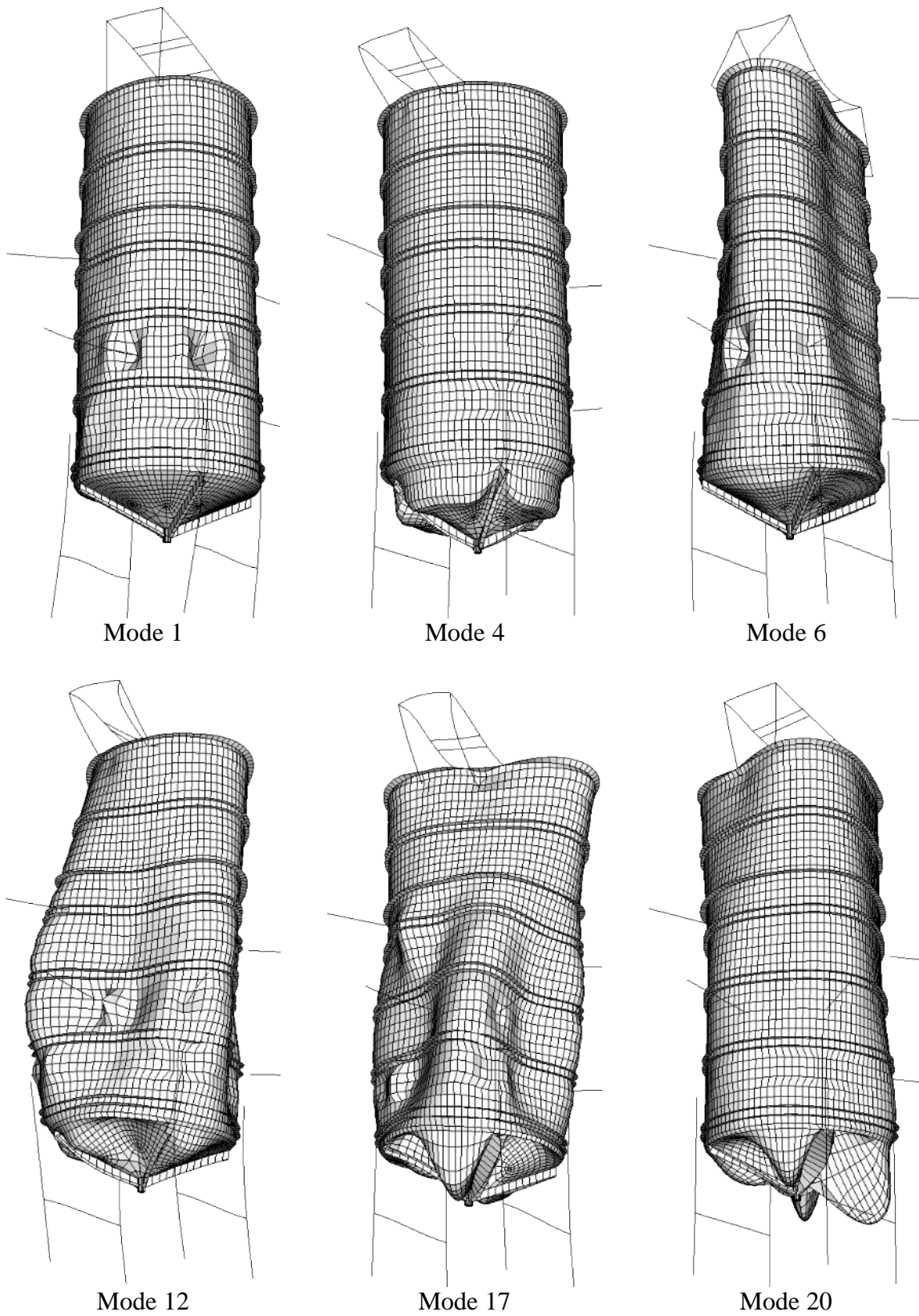


Figure 35. Selected eigenmodes of the pool with water. Note that Mode 4 is mainly vertical motion of the pool bottom caused by water.

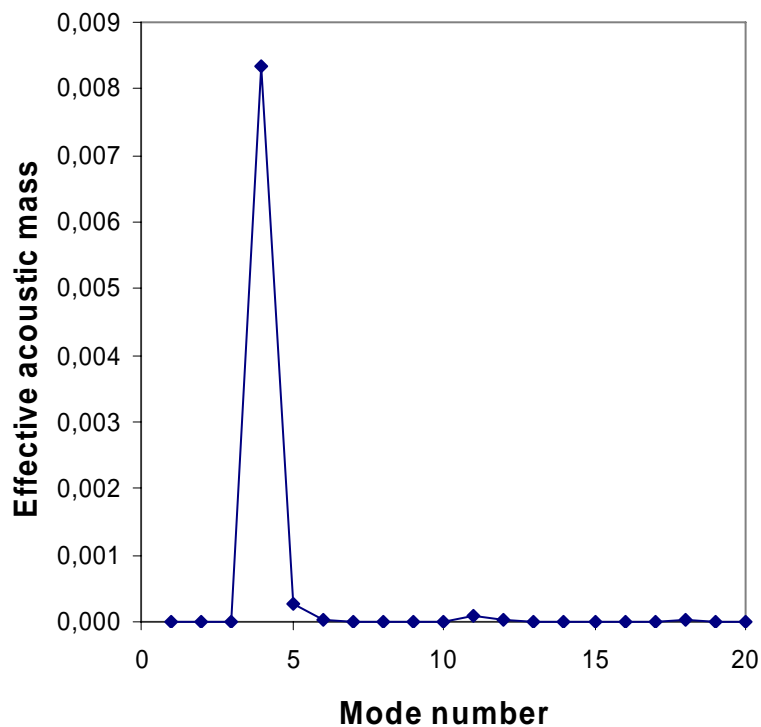


Figure 36. Effective acoustic mass for the first 20 eigenmodes of the pool in the coupled acoustic-structural analysis.

6 Summary and Conclusions

6.1 Method of Images

This work was a direct continuation to that done by Timo Narumo in 2004 (Pättikangas et al., 2005, pages 9-22). The main question that was left open at that time was how to determine the pressure source for the Method of Images (MOI). Another central question that arose during this work is whether the MOI is, in fact, an appropriate method for pressure load studies.

The first question, about value of pressure source, still remains open, although new information on the topic was gathered from various sources. The difficulty can be traced up to knowing the dynamics of a rapidly condensing steam bubble, which is not an easy task. This work remains theoretical, or literature-based, as no actual calculations were done due to the very short time available. Anyhow, the question of pressure source is independent of MOI, as any method of solving the Poisson equation requires the pressure source.

The other central question concerns the method of calculating pressure loads. At least the following main alternatives can be listed:

1. Analytical by using the appropriate Green's function for the actual geometry (Giencke, 1981).
2. The Method of Images.
3. A difference method (SILA) of solving the Poisson equation (Eerikäinen, 1997).

4. One-phase CFD calculation, modeling the collapsing bubble as a mass sink (Timperi et al., 2004).
5. Two-phase CFD calculation, detaching from the assumption of potential flow.

Alternatives 1-3 are methods of solving the Poisson equation, resulting from assumption of potential flow, whereas alternative 5 is the most general approach. As two-phase CFD is not mature yet, accurate results probably cannot be expected in near future. The method of Green's functions may be too complicated for arbitrary situations.

Certainly, the MOI is a serious method for estimation of the pressure loads, as it has been extensively used for that purpose for a long time. But when comparing the MOI and SILA, there seem to be several reasons to choose SILA:

- SILA is a documented code whose author is available at VTT.
- SILA calculates more accurately than the MOI in arbitrary geometries, because no rectangular-pool or similar approximation is needed.
- SILA is probably faster than the current moi.f code.

6.2 Homogeneous Two-phase Model

Earlier work carried out in this project with the homogeneous two-phase model was continued. In the present work, the model was implemented and tested in the new Fluent environment. According to the tests it seems that the very special characteristic of the homogeneous water/steam mixture makes it difficult or even impossible to implement the homogeneous two-phase model in the present day CFD codes.

According to video recordings of the POOLEX experiment, the steam-water surface remains reasonably smooth at least in the experiments where chugging oscillations occur. From the point of view of load calculations for pressure suppression pools, the chugging region is perhaps the most important one. Therefore, the two-phase modeling of steam and water will be continued by using the Volume Of Fluid (VOF) model which is suitable for situations where reasonably smooth surface exists between the phases. VOF model has so far only been used with some success for simulations of air and water. Addition of condensation model to the VOF model is therefore necessary. When the mass flux in blowdown is large, the two-phase mixture contains droplets and bubbles in addition to large regions of pure water and steam. Such situations can not be handled with current VOF models.

6.3 Coupled CFD and Structural Analyses

Two different solutions for coupling commercial CFD and structural analysis codes for FSI calculations of the water pool were tested. The MpCCI code was used with Fluent and the ES-FSI code was used with Star-CD. The ABAQUS FE code was used for the structure with both coupling methods.

FSI calculations of the pool were first attempted with two-directional coupling. However, numerical instabilities of the coupled system prevented the calculations from being done. Several test calculations with the MpCCI and ES-FSI codes were performed in order to overcome the instabilities, but with no positive results. Calculations of the pool were finally performed by using one-directional coupling. In the one-directional simulations with MpCCI, the incompressible and compressible VOF models of the new version of Fluent were used. With ES-FSI, the incompressible VOF model of Star-CD was used.

The VOF calculation with compressible air model led to clearly higher loads than calculations with incompressible air model. The velocity of the expelled water plug was in the compressible calculation two times as large as in the incompressible calculation. A longer section of the blowdown should, however, be included in the CFD model. The present model only contains the section starting at the level of the top of the water pool, which may to some extent affect the results of the compressible calculation. To our knowledge, all previous published VOF calculations have been done with incompressible model.

Results obtained with the one-directional ES-FSI simulation were compared to the modelled POOLEX experiment. Comparison of the steam-water interface in the simulation and experiment indicate that the condensation of steam was quite rapid in the modelled situation. This made the results of the simulation useless in the late phase of the blowdown. Two other main sources of error were probably the use of incompressible gas and one-directional coupling. The magnitudes of the pressure and stress peaks due to the water plug hit on the pool bottom were of comparable size in the simulation and experiment.

Similar difficulties with stability as the ones encountered in this work have been reported in the literature. The difficulties seem to arise commonly with incompressible and dense fluids (Causin et al., 2004; Anon., 2005b). These two properties were found to affect the stability considerably also in this work. Numerical stability of the coupled system obviously depends on the structure as well. The main remedy that has been used successfully is the use of implicit coupling (Causin et al., 2004; Matthies and Steindorf, 2002; Abouri et al., 2004). Adding compressibility of the fluid to the calculation may also make the calculation stable (Anon., 2005b). This increased stability also in the case of the pool considerably, although the compressibility of water is relatively small. In some cases it might be possible to use an artificially large compressibility for the fluid in order to obtain a stable calculation.

The overall coupling cycle of MpCCI and ES-FSI is explicit. Implicit coupling scheme is not available in either one of the coupling methods as such. This property sets limits to the stability of the overall integration scheme, and also limits the problems that can be solved. Fluid-structure interaction problems are often divided to problems with weak physical coupling and those with strong physical coupling. When the physical coupling is strong, either implicit overall integration scheme or simultaneous solutions of fluid and structural equations may be necessary. At least with MpCCI, it may be possible to implement implicit coupling by using for example the user subroutines of the coupled codes. This kind of solution was used by Abouri et al. (2004).

6.4 Coupled Acoustic-structural Analyses

Fluid-structure interaction analyses were also carried out entirely in ABAQUS. Fluid was modelled by using acoustic elements and the acoustic and structural domains were coupled. Eigenvalue extractions were carried out for two simple test cases and for the pool. Results obtained with ABAQUS were compared to analytical and experimental results. In the test cases, results calculated with other FE codes were also included for comparison. The effect of compressibility of the fluid was examined by comparing the results of the acoustic analyses to the results calculated with the assumption of incompressible fluid.

Agreement between the acoustic FE calculations and different reference calculations with compressible fluid was good. Eigenfrequencies with the assumption of incompressible fluid were higher compared to the frequencies obtained by using compressible fluid. However, the

results differed considerably only at high frequencies. For the two-dimensional test case, a condition which allows the use of incompressible fluid is presented in Yu (1987). The same condition is, however, probably applicable to a more general case.

In the case of the cylinder for which experimental results were available, the calculated and measured frequencies were close to one another for certain eigenmodes. The results for the empty cylinder indicate that the errors in the rest of the examined eigenfrequencies were due to inaccuracies in the structural model. For the pool, the calculated frequency of the predominant mode of oscillation was compared to the value indicated by the POOLEX experiments. The calculated frequency was clearly higher compared to the measured one. This was probably due to the too stiff pool bottom in the FE model. In spite of the above mentioned differences, the results indicate that the coupled acoustic-structural analysis can be used for calculating the coupled eigenmodes of a pressure suppression pool.

References

ABAQUS Theory Manual, 2004. Version 6.5. Hibbit, Karlsson & Sorensen Inc. RI.

Abouri, D., Parry, A., Hamdouni, A., 2004. A stable fluid rigid body interaction algorithm: application to industrial problems. ASME/JSME Pressure Vessels and Piping Conference **491-1**.

Anon., 2001. Star-CD Methodology, CD Adapco Group.

Anon., 2005a. Fluent 6.2 User's Guide, Fluent Inc., Lebanon, USA.

Anon., 2005b. Introduction to fluid-structure interaction simulation using ABAQUS and Fluent. 2005 ABAQUS users' conference, Stockholm, Sweden. ABAQUS Inc.

Calonius, K., Pättikangas, T. and Saarenheimo, A., 2003. Numerical analyses of a water pool under loading caused by large air and steam bubbles, VTT Industrial Systems, Project Report BTUO72-031106, Espoo, Finland, 43 p.

Causin, P., Gerbeau, J.-F., Nobile, F., 2004. Added-mass effect in the design of partitioned algorithms for fluid-structure problems. ICES report 04-02, The Institute for Computational Engineering and Sciences.

Eerikäinen, L., 1997. Potentiaaliteorian mukainen painejakauma nestealtaassa ja sen laskemiseen tarkoitettut SILA-tietokoneohjelmat. Käytönopas. (Pressure distribution in a pool of liquid according to potential theory, and the SILA computer codes for its calculation. User's guide.), VTT Energy, Technical report LVT-1/96, Espoo, Finland, 21 p. (in Finnish)

Giencke E., 1981. Pressure distribution due to a steam bubble collapse in a BWR pressure suppression pool. Nuclear Engineering and Design 65, 175-196.

Junger, M. and Feit, D., 1986. Sound, structures and their interaction. The MIT Press, Cambridge, Massachusetts.

Kerney, J., Feath, G. M. and Olson D. R., 1972. Penetration characteristics of a submerged steam jet, AIChE J., 18[3], 548-553.

Lahey, R. T. and Moody, F. J., 1993. The thermal hydraulics of a boiling water nuclear reactor, 631 p.

Laine, J., 2002. Condensation pool experiments with non-condensable gas. Research Report TOKE-2/2002, Lappeenranta University of Technology, Nuclear Safety Research unit, 46 p. + app. 14 p.

Laine J. and Puustinen M, 2003. Condensation pool preliminary experiments with steam. POOLEX 4/2003 research report, Lappeenranta Lappeenranta University of Technology, Nuclear Safety Research unit, 24 p. + app. 7 p.

- Laine J. and Puustinen M., 2005. Condensation pool experiments with steam using DN200 blowdown pipe. POOLEX 4/2004 research report, Lappeenranta University of Technology, Nuclear Safety Research unit, 41 p. + app. 4 p.
- Lamb, H., 1975. Hydrodynamics, Sixth Edition, Cambridge University Press.
- Matthies H., Steindorf, J., 2002. Partitioned but strongly coupled iteration schemes for nonlinear fluid-structure interaction. Institute of Scientific Computing, Technische Universität Braunschweig.
- Mazúch, T., Horá ek, J, Trnka, J. and Veselý, J., 1996. Natural modes and frequencies of a thin clamped-free steel cylindrical storage tank partially filled with water: FEM and measurement. Journal of Sound and Vibration **193**, No. 3, p. 669-690.
- MpCCI Technical Reference, 2005. Version 3.0. Fraunhofer Institute for Algorithms and Scientific Computing, Sankt Augustin, Germany, 168 pp.
- Niemi J., 2005, Homogeenisen kaksifaasimallin toteutus 3D simulointiympäristössä, draft.
- Puustinen, M., 2005a. Personal communication.
- Puustinen, M., 2005b. Unpublished document. Lappeenranta Lappeenranta University of Technology, Nuclear Safety Research unit.
- Pättikangas T., Raussi P., Pokela H. and Huttunen M., 2000. Two-dimensional CFD simulation of water hammer in a pool, VTT Energy, Espoo, Finland.
- Pättikangas, T. and Pokela H., 2003. Wall-loadings caused by large air bubbles injected in a water pool, VTT Processes, Project Report PRO4/T7534/02, Espoo, Finland, 28 p.
- Pättikangas T., Timperi A., Niemi J. and Narumo T., 2005. Fluid-structure interaction analysis of a water pool under loading caused by a condensation induced water hammer, VTT Industrial Systems, Research Report BTUO72-051332, Espoo, Finland, 56 p.
- Timperi A., Pättikangas T., Calonius K., Tuunanen J., Poikolainen J. and Saarenheimo A., 2004. Numerical analyses of a water pool under loadings caused by a condensation induced water hammer, VTT Industrial Systems, Research Report BTUO72-031198, Espoo, Finland, 66 pp.
- Tuomainen, M., 2001. Lauhdutusallaskokeiden suunnittelulaskuja Fluent-ohjelmalla, VTT Energia, Projektiraportti ENE4-PR-12/01, 22 pp.
- Wood B. D., Sun W-J. and Domoto G. A., 1980. Determination of pressure fields in a BWR suppression pool by means of Green's function and comparison with method of images and a finite difference solution. Nuclear Engineering and Design 61, 153-161.
- Yadigaroglu, G. and Lakehal, D., 2003. New challenges in computational thermal hydraulics, NURETH-10, Seoul, Korea, October 5-9, 2003.
- Youn, D. H., Ko, K. B., Lee, Y. Y., Kim, M. H., Bae, Y. Y. And Park, J. K., 2003. The direct contact condensation of steam in a pool at low mass flux, Nuclear Science and Technology, Vol. 40, No. 10, 881-885.

Yu, I.-W., 1987. Subspace iteration for eigensolution of fluid-structure interaction problems. *Journal of Pressure Vessel Technology* **109**, p. 244-248.

Title	Fluid-Structure Interaction Analysis of a Water Pool under Loading Caused by Steam Injection
Author(s)	Antti Timperi, Timo Pättikangas, Jarto Niemi and Mikko Ilvonen
Affiliation(s)	VTT Technical Research Centre of Finland
ISBN	87-7893-189-4 <i>Electronic report</i>
Date	April 2006
Project	NKS_R_2002_01 DeliPool
No. of pages	64
No. of tables	9
No. of illustrations	36
No. of references	31
Abstract	<p>Fluid-structure interaction (FSI) calculations were carried out by coupling CFD and structural analysis codes. MpCCI 3.0 was used for coupling Fluent CFD code with ABAQUS FE code. ES-FSI was used for coupling Star-CD CFD code with ABAQUS. FSI analyses, in which the calculation was carried out entirely in ABAQUS, were also performed. In this case, acoustic elements were used for the fluid and the acoustic and structural domains were coupled. FSI calculations were performed for simple test cases and for a test pool at Lappeenranta University of Technology. The Method of Images was studied as an alternative method for the analyses of the pool. Particularly, the determination of pressure source for the method was studied. Earlier work carried out with the homogenous two-phase model was continued by testing the model with Fluent. Calculation of condensation of steam in a water pool was tested with a new implementation.</p> <p>The two-directionally coupled simulations of the pool with MpCCI and ES-FSI were found to be numerically instable. It was concluded that an implicit coupling method may have to be used in order to avoid the instability. Calculations of the pool were finally performed by using one-directional coupling. In the simulations with MpCCI, the incompressible and compressible VOF models of Fluent were used. With ES-FSI, the incompressible VOF model of Star-CD was used for modelling the beginning of a steam injection experiment. The magnitudes of pressure and stress peaks in the simulation and experiment were of comparable size. Otherwise, however, differences between the simulation and experiment were large due to the simplifications used in the simulation. Results obtained with the acoustic-structural FE analyses were compared to analytical and experimental results. The results indicated that the coupled acoustic-structural analysis can be used for calculating the coupled eigenmodes of BWR pressure suppression pools.</p>
Key words	CFD, FE, fluid-structure interaction, steam injection, pressure suppression pool